LytM factors affect the recruitment of autolysins to the cell division site in *Caulobacter crescentus*

Aleksandra Zielińska [1,2,&,#], Maria Billini [1,2,#], Andrea Möll [1,2], Katharina Kremer [1], Ariane Briegel [3,4,§], Adrian Izquierdo Martinez [1,2], Grant J. Jensen [3,4], and Martin Thanbichler [1,2,5*]

[1]Faculty of Biology, Philipps-Universität, 35043 Marburg, Germany
[2]Max Planck Institute for Terrestrial Microbiology, 35043 Marburg, Germany
[3]Divison of Biological Engineering and [4]Howard Hughes Medical Institute, California Institute of Technology, Pasadena, CA 91125, USA
[5]LOEWE Center for Synthetic Microbiology, 35043 Marburg, Germany

[&]Current address: Faculty of Science and Engineering, University of Groningen, 9747 Groningen, Netherlands
[§]Current address: Sylvius Laboratorium, Leiden University, 2333 BE Leiden, Netherlands

[#] equal contributions

Key words:
Peptidoglycan hydrolases, SdpA, SdpB, AmiC, EnvC, NlpD, FtsEX

Running title:
The autolytic machinery of *C. crescentus*

[*]For correspondence:
E-mail: thanbichler@uni-marburg.de; Tel: (+49) 6421 2821809; Fax: (+49) 6421 2821832

ABSTRACT

Most bacteria possess a peptidoglycan cell wall that determines their morphology and provides mechanical robustness during osmotic challenges. The biosynthesis of this structure is achieved by a large set of synthetic and lytic enzymes with varying substrate specificities. Although the biochemical functions of these proteins are conserved and well-investigated, the precise roles of individual factors and the regulatory mechanisms coordinating their activities in time and space remain incompletely understood. Here, we comprehensively analyze the autolytic machinery of the alphaproteobacterial model organism *Caulobacter crescentus*, with a specific focus on LytM-like endopeptidases, soluble transglycosylases, and amidases. Our data reveal a high degree of redundancy within each protein family but also specialized functions for individual family members under stress conditions. In addition, we identify two lytic transglycosylases and an amidase as new divisome components that are recruited to midcell at distinct stages of the cell cycle. The midcell localization of these proteins is affected by two LytM factors with degenerate catalytic domains, DipM and LdpF, which may serve as regulatory hubs coordinating the activities of multiple autolytic enzymes during cell constriction and fission, respectively. These findings set the stage for in-depth studies of the molecular mechanisms that control peptidoglycan remodeling in *C. crescentus*.

INTRODUCTION

The bacterial cell wall is mainly made of peptidoglycan (PG), a heteropolymer composed of glycan chains with alternating β-1,4-linked *N*-acetylglucosamine (GlcNAc) and *N*-acetylmuramic acid (MurNAc) residues that are crosslinked by short peptide bridges (Höltje, 1998). The PG meshwork is constantly remodeled to enable cell growth, cell division, and adaptation of the cell to environmental conditions (den Blaauwen *et al.*, 2008). This task is accomplished by a large and redundant set of PG synthesizing and cleaving enzymes, whose activity needs to be closely coordinated to avoid lysis (Rice and Bayles, 2008; Typas *et al.*, 2012). The joint regulation of synthetic and lytic factors is facilitated by their assembly into multi-protein complexes. In the Gram-negative model species *Escherichia coli*, two of these complexes have been identified to date, namely the elongasome and the divisome, which mediate lateral and septal PG incorporation during cell elongation and cell division, respectively (den Blaauwen *et al.*, 2008; Uehara and Bernhardt, 2011; Typas *et al.*, 2012).

The PG-degrading enzymes (autolysins) of Gram-negative bacteria can be typically sorted into three main categories: enzymes that cleave the glycosidic bonds between MurNAc and GlcNAc (lytic transglycosylases), enzymes that hydrolyze the amide bond between MurNAc and its peptide side chain (amidases), and enzymes that separate the peptide bonds within and between the side chains (endo- and carboxypeptidases) (Vollmer *et al.*, 2008; van Heijenoort, 2011). In *E. coli*, the inactivation of single PG hydrolases does in most cases not cause any apparent phenotype. Notable exceptions are the DD-carboxypeptidases PBP5 (Nelson and Young, 2000) and PBP6b (Peters *et al.*, 2016), which are required for proper cell shape in standard or acidic growth conditions, respectively. However, the lack of multiple members from either the same or different functional groups often leads to severe morphological and growth defects. For instance, combined inactivation of the three amidases AmiA, AmiB, and AmiC largely blocks the cleavage of septal PG, leading to the formation of long chains of cells in which separated cytoplasms are surrounded and connected by a shared PG layer (Heidrich *et al.*, 2001; Priyadarshini *et al.*, 2007). Similarly, inactivation of six lytic transglycosylases leads to a mild chaining phenotype, whereas cells lacking multiple endopeptidases exhibit general cell shape defects (Heidrich *et al.*, 2002). Notably, there is functional cooperativity between PG hydrolases with distinct cleavage specificities. For example, the cell division defect of *E. coli* amidase mutants is aggravated by additional mutation of lytic transglycosylases and/or endopeptidases, indicating that all of these factors contribute to the cleavage of septal PG, albeit to varying extents (Heidrich *et al.*, 2002; Priyadarshini *et al.*, 2006).

Apart from their direct role in PG remodeling, autolysins have a critical role in antibiotic susceptibility. This is particularly true for lytic transglycosylases, because their catalytic activity generates anhydromuropeptides, which in *E. coli* stimulate the production of the beta-lactamase

AmpC, leading to elevated resistance against beta-lactam antibiotics (Jacobs *et al.*, 1994; Korsak *et al.*, 2005). Moreover, proper lytic transglycosylase and amidase activity is important to ensure the integrity of the outer membrane and, thus, protect the cell against large antibiotics such as vancomycin (Heidrich *et al.*, 2002; Korsak *et al.*, 2005). Even though the inhibition of PG hydrolases may increase sensitivity to antibiotics, it can on the other hand also confer resistance to lytic antibiotics by delaying the autolytic process (Rice and Bayles, 2008).

The mechanisms controlling the activity of autolysins are still incompletely understood. Among the well-studied examples are the regulatory pathways involved in the activation of the three amidases of *E. coli*. Their function in final septum cleavage is dependent on two divisome-associated metallo-peptidase homologs, EnvC and NlpD, which are characterized by a catalytically inactive LytM (M23) peptidase domain (Uehara *et al.*, 2010). This domain interacts with cognate amidases and induces a conformational change that removes an autoinhibitory α-helix covering the active site, thus activating their hydrolytic activity (Yang *et al.*, 2012; Peters *et al.*, 2013). The stimulatory effect of EnvC, in turn, relies on FtsE and FtsX, two divisome components that form a membrane-integral ATP-binding cassette transporter-like complex modulating the conformation of EnvC in an ATPase-dependent manner (Yang *et al.*, 2011). A similar regulatory effect of FtsEX and catalytically inactive LytM factors on the activity of autolysins has also been observed in other bacterial species (Meisner *et al.*, 2013; Sham *et al.*, 2013; Mavrici *et al.*, 2014; Möll *et al.*, 2014).

To date, most of the knowledge on autolysins in Gram-negative bacteria is based on studies in the gamma-proteobacterium *E. coli* (Vollmer *et al.*, 2008). However, recently, significant progress has also been made in several other proteobacterial species (Dominguez-Gil *et al.*, 2016; Alcorlo *et al.*, 2017). These studies revealed that the mechanisms identified in the prototypic *E. coli* system are not necessarily conserved in other bacterial lineages. One of the morphologically most diverse groups of bacteria are the alpha-proteobacteria (Randich and Brun, 2015), including the species *Caulobacter crescentus*, a well-established model for asymmetric cell division and cell polarity. *C. crescentus* is characterized by a dimorphic life cycle, in which a non-replicative motile swarmer cell differentiates into a sessile stalked cell that initiates chromosome replication, elongates and then divides to produce a stalked and a new swarmer sibling (Brown *et al.*, 2009). Cell elongation initially occurs by dispersed incorporation of new cell wall material, governed by the actin-like cytoskeletal protein MreB. After assembly of the divisome, the cell switches to divisome-dependent zonal growth at the cell center before it finally constricts to generate the two new daughter cells (Figge *et al.*, 2004; Dye *et al.*, 2005; Aaron *et al.*, 2007; Randich and Brun, 2015). Concomitant with cell elongation, a stalk is formed by zonal growth at the old cell pole (Aaron *et al.*, 2007). The dynamics of the cytoskeletal structures and regulatory complexes directing these different modes of growth in *C. crescentus* have

been investigated in appreciable detail (Gitai *et al.*, 2004; Dye *et al.*, 2005; Thanbichler and Shapiro, 2006 33; Alyahya *et al.*, 2009; Möll and Thanbichler, 2009; Kühn *et al.*, 2010; Goley *et al.*, 2011). However, the knowledge of the PG remodeling enzymes they control is still very limited. Studies of the synthetic machinery showed that, like in other model bacteria, the highly conserved transpeptidases PBP2 and PBP3 are essential for cell elongation and division, respectively (Dye *et al.*, 2005; Costa *et al.*, 2008). In addition, *C. crescentus* was found to contain five bifunctional penicillin-binding proteins with highly redundant functions (Yakhnina and Gitai, 2013; Strobel *et al.*, 2014), two of which are enriched at the cell divison site (Strobel *et al.*, 2014). A third member of this family interacts with the pole-associated bactofilin cytoskeleton to support stalk biogenesis (Kühn *et al.*, 2010).

Besides the PG synthases, a LytM domain-containing endopeptidase homolog, DipM, was shown to be critical for proper PG biosynthesis in *C. crescentus*. DipM is a soluble periplasmic protein that is recruited to the cell division site during early stages of the division process. Its inactivation leads to cell filamentation, delayed constriction of the outer layers of the cell envelope, and outer membrane blebbing (Goley *et al.*, 2010; Möll *et al.*, 2010; Poggio *et al.*, 2010). Notably, DipM possesses a degenerate catalytic domain and accordingly lacks hydrolytic activity. Its properties thus resemble those of EnvC and NlpD from *E. coli* (Uehara *et al.*, 2010) and *Vibrio cholerae* (Möll *et al.*, 2014), which mediate cell separation by stimulating amidase activity. Analysis of the *C. crescentus* genome sequence revealed only a single predicted amidase, named AmiC (Marks *et al*, 2010). However, the role of this protein and its functional relationship to DipM are still uninvestigated. In addition to DipM, the *C. crescentus* genome encodes six more putative endopeptidases of the LytM (M23) family and four putative soluble lytic transglycosylases (SLTs). One of the SLTs, PleA, has previously been implicated in pili and flagella biogenesis (Viollier and Shapiro, 2003), whereas the role of the remaining proteins has not been investigated so far.

In the present study, we comprehensively analyze the physiological roles of LytM factors and SLTs in *C. crescentus*. The characterization of mutants with defects in single or multiple hydrolases reveals a high degree of functional redundancy within each protein family but also specialized roles for individual members under non-standard conditions. Importantly, the most severe phenotypes are observed upon inactivation of DipM or a newly identified catalytically inactive LytM factor, called LdpF. Combined inactivation of these two proteins strongly reduces cell viability, and depletion of DipM in cells lacking all catalytically active LytM factors or all SLTs is synthetically lethal. Importantly, we show that two SLTs and AmiC localize to the division site in consecutive phases of the constriction process. Their recruitment to midcell is abolished or significantly impaired in cells deficient in DipM or LdpF, indicating a role for the two LytM factors in the spatiotemporal regulation of autolysin

function. However, the morphological defects induced by the lack of DipM or LdpF are different from those observed after inactivation of their putative target proteins. Collectively, DipM and LdpF may thus serve as regulatory hubs that help coordinate the activities of multiple autolysins at distinct stages of the cell cycle.

RESULTS

The LytM domain-containing protein LdpF is required for proper cell division

Apart from DipM, the *C. crescentus* genome encodes six more LytM factors (Goley *et al.*, 2010; Möll *et al.*, 2010; Poggio *et al.*, 2010), now called LdpA-F (*L*ytM *d*omain-containing *p*rotein A-F; **Tab. S1**). Whereas LdpA contains a putative N-terminal transmembrane helix, all of its paralogs feature predicted cleavable signal peptides, suggesting that they are soluble periplasmic proteins (**Fig. 1A**). Notably, DipM contains four N-terminal PG-binding LysM-domains that are critical for its localization to the division site (Goley *et al.*, 2010; Möll *et al.*, 2010; Poggio *et al.*, 2010). In contrast, most of its homologs do not feature any known functional domains apart from their C-terminal LytM domains, with the exception of LdpF, which contains two predicted coiled-coil motifs. A comparison of the LytM domain sequences (**Fig. S1A**) reveals that, similar to DipM, LdpF lacks several conserved residues that typically constitute the active site of LytM-like metallopeptidases (Bochtler *et al.*, 2004). One of the active-site residues involved in coordination of the metal cofactor is also altered in LdpB, but it is unclear whether this mutation (His → Cys) affects the catalytic activity of the protein. The remaining Ldp proteins appear to have fully functional LytM (M23) domains and may thus be genuine endopeptidases.

To investigate the importance of LdpA-F in *C. crescentus*, we generated mutants carrying single or multiple in-frame deletions in the corresponding genes. Most single mutants largely showed wild-type morphology, with no or only marginal changes in cell length and width (**Fig. S1B and C**). The only exception was the strain lacking *ldpF*, which displayed a noticeable cell separation defect. As a consequence, about 2.3% of cells in a Δ*ldpF* population exhibited a chaining phenotype, comprising more than two compartments that were separated by deep constrictions (**Fig. 1B and S1D**). Similar to the single mutants, strains carrying multiple deletions in the *ldpA-E* genes (data not shown) and even a Δ*ldpABCDE* quintuple mutant barely showed any morphological aberrations. However, additional deletion of *ldpF* in the Δ*ldpABCDE* background again caused an obvious chaining phenotype, reminiscent of that observed for the Δ*ldpF* single mutant (**Fig. 1B and C**). Notably, despite the lack of all *ldp* genes, cells still displayed wild-type growth rates (**Fig. S1E**). To examine the division defect of the *ldpF* mutant in more detail, we visualized constricted regions in separating chained cells by electron cryo-tomography. This analysis revealed that adjacent cell compartments had separate cytoplasmic spaces but were still connected by a thin tube made of PG, outer membrane and surface layer, indicating a delay in the final separation of the outer cell envelope layers (**Fig. 1D**). Thus, LdpF turns out to be another LytM factor with a role in *C. crescentus* cell division, whereas the biological role of the remaining Ldp proteins remains unclear. Importantly, there are clear differences between

the phenotypes of LdpF- and DipM-deficient cells (**Fig. 1B and Fig. 2**) (Goley *et al.*, 2010; Möll *et al.*, 2010; Poggio *et al.*, 2010), suggesting that the two proteins act in distinct cellular pathways.

As a means to further characterize the physiological roles of LdpA-F, we examined the sensitivity of various Ldp mutant strains to cell envelope stress. Previous work has revealed that *C. crescentus* exhibits very low salt tolerance (Hocking *et al.*, 2012). Consistent with this finding, we observed that wild-type cells developed significant morphological defects when grown in standard rich (PYE) medium containing more than 0.3% sodium chloride (data not shown). Spot assays showed that the wild type and most *ldp* mutants, including the Δ*ldpABCDE* quintuple mutant, grew normally on solid medium containing this threshold concentration of salt. In contrast, strains lacking *ldpF* consistently displayed a dramatic decrease in viability under these conditions (**Fig. 1E**), suggesting that LdpF is required to ensure the integrity of the cell envelope on exposure of the cells to ionic stress. Importantly, deletion of *dipM* did not affect halotolerance, again suggesting distinct functions for LdpF and DipM. To characterize the salt-induced defects of the *ldpF* mutant in more detail, we investigated the immediate response of exponentially growing wild-type and Δ*ldpF* cells to a sudden increase in the salt concentration. In case of the wild type, addition of sodium chloride led to a brief slow-down of growth, but the cells soon continued to proliferate at their normal rate, with no apparent change in morphology (**Fig. 1F-H**). The Δ*ldpF* mutant, by contrast, showed a significant decrease in its growth rate, accompanied by a conspicuous cell division defect. Consistent with the above findings, LdpF may thus have a specific role in cell division that is critical for proper growth under salt stress.

To clarify the localization patterns of LdpA-F, we generated derivatives of all six proteins carrying C-terminal fluorescent protein (mCherry) tags, synthesized under the control of a xylose-inducible promoter. However, in all cases, the full-length fusion proteins were undetectable by Western blot analysis due to cleavage of the fluorescent tag, preventing further analysis (data not shown).

DipM and LdpF have distinct roles in cell division and cell wall integrity

Our mutant analysis indicates that LdpF is involved in the late stages of cell division, even though its LytM domain is likely to be catalytically inactive. Previously, LytM factors with degenerate active sites were shown to control the activity of PG hydrolases, but the number of these regulatory factors and their target specificities vary between species (Uehara *et al.*, 2010; Möll *et al.*, 2014; Stohl *et al.*, 2015; Yakhnina *et al.*, 2015). To investigate the functional relationship between LdpF, DipM and the potentially catalytically active endopeptidases LdpA-E, we studied the effect of DipM depletion in various *ldp* mutant backgrounds. Spot assays revealed that DipM depletion had

combined absence of LdpF and DipM led to a strong reduction in cell viability, even though the growth behavior of strains lacking only one of these proteins was similar to that of the wild-type

strain (Fig. 2A). This synthetic effect supports the notion that LdpF and DipM act in distinct, but partially redundant pathways whose function is indispensable for proper cell division. Interestingly, an even stronger synthetic phenotype was observed in the Δ*ldpABCDE* background. Thus, while LdpA-E are largely redundant in the wild-type background, the putative hydrolytic activity of one or more of these proteins becomes critical upon inactivation of the DipM pathway. Importantly, cells depleted of DipM were barely viable when they lacked both the *ldpA-E* and *ldpF* genes (Δ*ldpABCDEF*), indicating that LytM factors are essential for growth in *C. crescentus*.

To further investigate the defects induced by the lack of LytM factors, *ldp* mutants were depleted of DipM during cultivation in liquid medium (Fig. S2) and analyzed for changes in their cell morphologies. Under these conditions, the lack of DipM only moderately affected the growth dynamics of Δ*ldpF* cells. However, consistent with the results of the spot assays, a considerable decrease in both growth rates and yields was observed for the Δ*ldpABCDE* and, even more so, for the Δ*ldpABCDEF* background (Fig. 2B). Microscopic analysis confirmed that depletion of DipM in an otherwise wild-type background yielded slightly swollen, elongated and chained cells with shallow constrictions (Fig. 2C). Additional deletion of *ldpF* aggravated the chaining phenotype, leading to a significant increase in average cell length without major changes in cell width (Fig. 2D). In the Δ*ldpABCDE* background, by contrast, DipM depletion resulted in considerably greater cell widths but barely any change in cell length, yielding short, swollen, and irregularly shaped filaments. Interestingly, an additive phenotype was observed after reduction of the DipM levels in cells carrying mutations in both *ldpF* and *ldpABCDE*, as reflected by the formation of short chains of swollen, irregularly shaped cells. These results support a role of LdpF in cell separation, and they suggest that the presence of DipM and one or more of the Ldp endopeptidases is required for the proper control of cell width.

SLTs are required for multiple aspects of cell envelope integrity

Given the synthetic phenotypes obtained after combined inactivation of LytM factors with degenerate and authentic LytM domains, we conclude that LdpF and DipM are unlikely to act mainly through stimulation of the catalytically active endopeptidases LdpA-E. To further dissect the interplay between the components of the autolytic machinery of *C. crescentus*, we turned our attention to the SLTs, a second family of hydrolases with key functions in cellular PG metabolism. In addition to PleA (Viollier and Shapiro, 2003), the *C. crescentus* genome encodes three proteins with an SLT domain, now called SdpA-C (*S*LT *d*omain-containing *p*rotein A-C; Tab. S1). SdpA-C all feature a predicted cleavable signal sequence, suggesting that they are soluble periplasmic proteins (Fig. 3A). PleA, by contrast, does not contain any apparent signal sequence or transmembrane helix, suggesting that it may be secreted to the periplasm by a so-far unknown mechanism (Viollier and Shapiro, 2003).

To investigate the function of SLTs in *C. crescentus*, we first constructed various deletions in the *sdp* genes and analyzed the morphology of the resulting strains. Single and double mutants largely showed wild-type morphology, although some of them exhibited moderate changes in cell length and width (**Fig. S3**). Similarly, the Δ*sdpABC* triple mutant only had minor growth defects, with a small fraction of elongated and/or chained cells (**Fig. 3B and C**). A slightly stronger cell elongation phenotype was observed for a strain that additionally lacked PleA, indicating that this protein may not only function in pili biogenesis but also in more general aspects of cell wall biogenesis. Notably, despite their morphological defects, all of the mutant strains displayed wild-type viability (**Fig. 3D**) and growth rates (data not shown). Close examination of light microscopic images indicated that, in addition to their cell length phenotype, Δ*sdpABC* cells frequently formed membranous protrusions, in particular at the cell poles and the stalk (**Fig. 3E**). To clarify the nature of these structures, we labeled the periplasmic space of the triple mutant using a red fluorescent protein derivative with an engineered signal sequence that mediates secretion of the protein via the twin-arginine translocation (Tat) pathway (Palmer and Berks, 2012). Fluorescence imaging revealed a strong accumulation of the fluorescent label in the protrusions, suggesting a defect in the integrity of the cell envelope that leads to the formation of outer membrane blebs (**Fig. 3E**). This hypothesis was confirmed by electron cryo-tomographic analysis of Δ*sdpABC* cells (**Fig. 3F**). Virtual sections through the polar and midcell regions showed large local expansions of the periplasmic space, resulting from the loss of association between the cytoplasmic membrane and the outer layers of the cell envelope. Thus, SLT activity appears to be required for cell envelope integrity and/or proper outer membrane homeostasis, potentially by modulating the properties of the PG layer.

SdpA and DipM are necessary for β-lactam resistance

Previous studies have shown that SLTs play an important role in antibiotic sensitivity. In *E. coli* and its relatives, for instance, anhydromuropeptides generated by SLTs are required to induce synthesis of the β-lactamase AmpC and, thus, confer β-lactam resistance (Jacobs *et al.*, 1994; Korsak *et al.*, 2005; Zeng and Lin, 2013). On the other hand, SLTs critically contribute to the lysis of cells after the inhibition of transpeptidase activity by β-lactam antibiotics (Cho *et al.*, 2014).

C. crescentus possesses a potent β-lactamase (Mbl1b) that renders it intrinsically resistant to high levels of β-lactam antibiotics (Simm *et al.*, 2001; West *et al.*, 2002). To test for a role of PG hydrolases in the resistance mechanism, we determined the viability of various hydrolase mutants on solid media containing the β-lactam ampicillin. Spot assays revealed that cells lacking most of the predicted endopeptidase homologs (Δ*ldpABCDEF*) showed the same degree of resistance as the wild-type strain (**Fig. 4A**). However, a strong decrease in viability was observed for the Δ*dipM* and, even more so, the Δ*sdpABC* mutant. To more precisely define the SLTs responsible for this effect, the same

analysis was repeated with a set of strains lacking all possible combinations of *sdp* genes (**Fig. 4B**). Interestingly, all mutants lacking *sdpA* turned out to be ampicillin sensitive, whereas deletions in *sdpB* and/or *sdpC* had no effect. Thus, DipM and SdpA appear to be required for high-level β-lactam resistance.

Given the role of SLTs in the regulation of β-lactamase gene expression in *E. coli*, it was conceivable that Δ*dipM* and Δ*sdpA* cells failed to generate a specific PG degradation intermediate involved in Mbl1b induction. To test this hypothesis, we analyzed the mutant strains for their ability to hydrolyze nitrocefin, a chromogenic cephalosporin derivative commonly used to detect β-lactamase activity (**Fig. 4C**). Interestingly, all of the hydrolase mutants were still capable of turning over nitrocefin with the same efficiency as the wild-type strain, whereas no hydrolysis was observed for a control strain lacking Mbl1b (Δ*bla*). We further observed that the levels of β-lactamase activity were independent of the presence of antibiotic in the growth medium (**Fig. 4C and S4A**). Thus, SLTs or DipM do not appear to be required for proper β-lactamase gene expression. Instead, they may potentially help to compensate for the inactivation of other, highly β-lactam-sensitive PG synthases or hydrolases (Vollmer *et al.*, 2008), whose function is redundant under standard growth conditions.

To further investigate the effect of ampicillin on PG hydrolase mutants, we cultivated cells in liquid medium and monitored their response to sub-lethal concentrations of the antibiotic. Both wild-type and Δ*sdpA* cells continued to grow after the addition of ampicillin, although their doubling times were slightly decreased (**Fig. S4B**). However, whereas the morphology of the wild type remained unchanged, the mutant cells failed to divide efficiently, leading to a significant increase in cell length (**Fig. 4D and E**). These data support the notion that SdpA contributes to PG remodeling during cell division and complements the activity of another division-related factor that is inhibited by ampicillin despite the presence of Mbl1b. Of note, under the conditions used, the Δ*dipM* mutant did not show any additional growth and cell shape defects (**Fig. S4B**; data not shown), indicating that it may only be sensitive to higher β-lactams concentrations, as used in the spot assay.

SdpA, SdpB, and AmiC localize to midcell at distinct stages of the division process

The results of our mutant analysis point to a role for LdpF and SLTs in PG remodeling during cell division. To further corroborate this notion, we set out to determine the subcellular localization patterns of SdpA-C and clarify whether they accumulate at the division site. For this purpose, we generated fusion constructs carrying a C-terminal red fluorescent protein (mCherry) tag and expressed the corresponding alleles in the wild-type background under the control of a xylose-inducible promoter. However, after induction, only SdpA-mCherry and SdpB-mCherry were detectable as full-length proteins by Western blot analysis (**Fig. S5**), whereas the SdpC-containing construct was quantitatively cleaved within the linker connecting the fusion partners (data not

shown). Microscopic analysis of cells producing the two stable constructs revealed that both SdpA-mCherry and SdpB-mCherry showed cell cycle-dependent localization patterns. In swarmer cells, both proteins were evenly distributed within the cell envelope (**Fig. 5A and B**). Shortly after transition to the stalked-cell stage, they then relocated to the incipient division site, forming a diffuse band that gradually condensed into a tight focus as the cell constricted. This localization behavior was similar to that observed for DipM (Möll *et al.*, 2010). However, unlike DipM, both proteins were released from midcell during the final stages of the division process and thus, in large part, evenly distributed again before final separation of the daughter cells. These results demonstrate that SdpA and SdpB are indeed components of the cell division machinery in *C. crescentus* that may mainly contribute to constriction but possibly not to final fission of the cell.

Given the role of LytM factors with degenerate peptidase domains in the stimulation of amidase activity, it was conceivable that LdpF or DipM could be functionally related to the only predicted amidase of *C. crescentus*, AmiC. We therefore also performed localization studies of an inducible AmiC-mCherry fusion to test for its recruitment to the division plane (**Fig. 5C**). Throughout most of the cell cycle, the protein was evenly distributed in the cell envelope. However, towards the end of the division process, it consistently condensed into a bright focus at the site of constriction, which persisted until cytokinesis was completed. Hence, AmiC is also part of the division apparatus and likely involved in the final separation of the two daughter cells.

To determine the rank of SdpA, SdpB, and AmiC in the hierarchy of divisome assembly, we compared their localization dynamics with those of the well-characterized divisome components FtsZ, FtsN, and TipN (Huitema *et al.*, 2006; Thanbichler and Shapiro, 2006; Möll and Thanbichler, 2009). To this end, we followed synchronized cells producing suitable fusion proteins over the course of one cell cycle and quantified the fraction of cells exhibiting a fluorescent focus at midcell as a function of time (**Fig. 5D**). Interestingly, SdpA and SdpB showed a localization behavior very similar to that of FtsN, an essential cell division protein that plays a central regulatory role in the orchestration of cell constriction (Weiss, 2015). AmiC, by contrast, relocated to the division site at a much later time point, shortly before TipN, the latest recruit to the divisome identified in *C. crescentus* so far (Goley *et al.*, 2011). To determine whether the recruitment of the two SLTs was dependent on FtsN, their localization was reinvestigated in a conditional *ftsN* mutant (**Fig. S6A and B**). In the absence of FtsN synthesis, cells developed into long, smooth filaments, with both SdpA-mCherry and SdpB-mCherry evenly distributed throughout the cell envelope. After a shift to inducing conditions, these filaments started to resume cell division. Concurrently, the fusion proteins condensed into distinct foci at the division sites that dispersed again before final separation of the daughter cells. These data confirm that the

two SLTs require FtsN for their recruitment to midcell, suggesting that they could be part of the FtsN-regulated machinery mediating the remodeling of PG at the cell division site.

DipM and LdpF are required for proper midcell localization of SdpA, SdpB, and AmiC

Our results show that DipM and LdpF are both involved in cell division, although they likely function in different pathways. Considering that LytM factors with degenerate peptidase domains usually serve as regulators of genuine PG hydrolases, we aimed to investigate the interplay of the two proteins with division-related components of the lytic machinery in *C. crescentus*. To this end, we first asked whether deletion of *dipM* would affect the localization behavior of fluorescently tagged SdpA, SdpB, and AmiC derivatives. In the mutant cells, both SdpA-mCherry and SdpB-mCherry indeed failed to condense at midcell and were evenly distributed throughout the cell envelope (**Fig. 6A and B**). The localization behavior of AmiC-mCherry, on the other hand, was unchanged under these conditions (**Fig. S7A**). Thus, DipM appears to be required, directly or indirectly, to recruit SdpA and SdpB to the cell division site. In the Δ*ldpF* background, by contrast, the two SLTs showed the same subcellular distribution as in the wild-type strain (**Fig. S7B and C**). However, in this case, AmiC-mCherry only formed very faint midcell foci, and a large fraction of the protein remained delocalized (**Fig. 6C**). Western blot analysis verified that the effects observed were not due to changes in the levels or stability of the fusion proteins (**Fig. S5**). Collectively, these results point to a role of DipM and LdpF in the midcell recruitment of autolysins in *C. crescentus*.

Inactivation of AmiC or SdpABC strongly reduces the viability of LdpF- or DipM-deficient cells

Having identified a connection between non-canonical LytM factors and certain PG remodeling enzymes at the level of protein localization, we aimed to analyze the functional relationship between these proteins in more detail using epistasis analysis. For this purpose, we first attempted to combine deletions in the *ldpF* and *amiC* genes. However, it turned out to be impossible to delete *amiC* in the absence of a complementing construct, both in the Δ*ldpF* and the wild-type background. In line with results obtained by large-scale transposon mutagenesis (Christen *et al.*, 2011), the amidase activity of AmiC thus appears to be essential for viability in *C. crescentus*. To further investigate the role of AmiC, we generated conditional mutants expressing *amiC* under the control of a xylose-inducible promoter. In a strain carrying an intact *ldpF* gene, depletion of AmiC had no obvious effect on cell viability (**Fig. 7A and B**), suggesting that basal levels of amidase activity are sufficient for growth. Consistent with this notion, uninduced cells only showed mild morphological aberrations, such as a moderate elongation of the cell bodies (> 4.2 µm; 31% of the population; n = 339) and chaining (**Fig. S8**). In the Δ*ldpF* background, by contrast, a decrease in AmiC levels caused a drastic reduction in cell viability, combined with a strong decrease in the growth rate and a high incidence of elongated (63%; n = 339) or chained cells (**Fig. 7 and S8**). Notably, the compartments of chained cells were

frequently connected by thin tubular structures, indicating a block at the final stages of cell division, shortly before membrane fusion. This strong synthetic effect, together with the essentiality of AmiC, suggests that the role of LdpF cannot lie exclusively in the control of AmiC function.

Focusing on the interrelation of DipM and SLTs, we next attempted to delete the *dipM* gene in Δ*sdpABC* cells. As this was not possible, we resorted to the use of conditional mutants in which the expression of *dipM* was placed under the control of a xylose-inducible promoter. Spot assays on solid media showed that neither Δ*sdpABC* nor Δ*sdpABC* Δ*pleA* cells were viable when grown under non-inducing conditions, indicating that DipM is essential in these mutant backgrounds (**Fig. 8A**). To clarify the reasons underlying this growth defect, we cultivated the two mutant strains in liquid medium and monitored their growth and morphology during the course of DipM depletion. Consistent with the results of the spot assay, both strains ceased to grow shortly after their transfer to inducer-free medium (**Fig. 8B**). Concomitantly, the cells developed into short filaments with lengths similar to those observed after depletion of DipM in an otherwise wild-type background. Importantly, however, these filaments lacked stalks, displayed significantly larger cell widths, and formed abundant outer membrane blebs (**Fig. 8C and D**), indicative of a severe defect in cell envelope integrity. The synthetic phenotypes obtained after combined inactivation of DipM and SLTs indicate that these proteins affect PG remodeling, at least in part, through separate pathways, consistent with the phenotypic differences observed for DipM- and SLT-deficient cells (**Fig. 1 and 3**). However, since DipM is required to position SdpA and SdpB at midcell, the defects caused by DipM depletion may, to some extent, originate from a reduced activity of SLTs in the delocalized state.

DISCUSSION

This work represents the first comprehensive analysis of the autolytic machinery in *C. crescentus*, with a focus on the contributions of LytM-like endopeptidases and soluble lytic transglycosylases to cell growth and division. Our data reveal a high degree of functional redundancy within each protein family but also specialized activities for individual family members under certain non-standard growth conditions. In addition, we provide new insight into the physiological roles of two non-canonical LytM-like endopeptidase homologs, DipM and LdpF, by dissecting their functional interactions with other lytic proteins and identifying potential regulatory targets.

PG from *C. crescentus* is characterized by an unusually high content of 1,6-anhydro-muropeptides, indicating a high level of lytic transglycosylase activity that may be critical for establishing the complex cell shape of this species (Takacs *et al.*, 2010). We show that the inactivation of multiple SLTs indeed leads to an impairment of cell division and cell envelope integrity. The chaining phenotype of the Δ*sdpABC* (Δ*pleA*) mutant is reminiscent of the defects observed for SLT-deficient *E. coli* (Heidrich *et al.*, 2002) and *Staphylococcus aureus* (Stapleton *et al.*, 2007) cells, suggesting a conserved function for SLTs in the remodeling of septal PG. This notion is supported by the finding that, in *C. crescentus*, at least two of the SLTs are recruited to the division site, indicating a specific role for them in cell constriction. However, overall, the morphological defects observed for the Δ*sdpABC* Δ*pleA* mutant are relatively mild, which may be explained by the fact that *C. crescentus* additionally contains four predicted membrane-bound lytic transglycosylases (Marks *et al.*, 2010) that may partially compensate for the loss of SLT activity. Apart from their cell division defect, Δ*sdpABC* cells show a pronounced tendency to shed outer membrane vesicles. This observation suggests that certain PG modifications introduced by SLTs are required to stably anchor the outer cell envelope to the cell wall. Alternatively, reduced SLT activity may lead to an increase in the thickness of the PG layer that entails the loss of contacts between the inner and outer membrane, as mediated for instance by the conserved Tol-Pal complex (Gerding *et al.*, 2007; Yeh *et al.*, 2010). Interestingly, despite the high functional redundancy of SLTs, we identified a specific role for SdpA in high-level β-lactam resistance. Since the Δ*sdpA* mutant retains wild-type β-lactamase activity, we suggest that cells lacking SdpA are hypersensitive to reduced transpeptidase or carboxypeptidase activity resulting from the residual levels of antibiotic that escapes degradation by Mbl1b. The specificity of this effect for a single protein indicates that different SLTs may have distinct substrate preferences or activity patterns. This notion is supported by the previous finding that PleA is specifically required for proper pilus biogenesis (Viollier and Shapiro, 2003). However, more detailed analyses are required to fully unravel the contributions of SLTs to cell wall biogenesis in *C. crescentus*.

Unlike the inactivation of SLTs, the loss of all five authentic LytM-like endopeptidases (LdpA-E) does not produce any noticeable phenotype, suggesting that these proteins may have a redundant and more general function in cell growth. In contrast, obvious cell division and cell shape defects were observed for cells lacking the non-canonical LytM factors DipM or LdpF, which are characterized by degenerate peptidase domains with defective catalytic sites. Previous work has confirmed that DipM indeed lacks appreciable hydrolytic activity *in vitro*. Nevertheless, it is required for proper cell division, with its loss leading to delayed invagination of the outer envelope layers due to aberrant remodeling of the cell wall during cell constriction (Goley *et al.*, 2010; Möll *et al.*, 2010; Poggio *et al.*, 2010). Collectively, these findings indicate that DipM may serve as a hub for other PG biosynthetic proteins at the division site, but its precise mode of action and its potential regulatory targets have remained unknown. Studies in *E. coli* and *V. cholerae* demonstrated that catalytically inactive LytM factors can control the activity of N-acetylmuramoyl-L-alanine amidases (Uehara *et al.*, 2010; Möll *et al.*, 2014). However, the phenotypic consequences of DipM and AmiC depletion are clearly different. Moreover, the two proteins are recruited to midcell at distinct stages of the division process, with AmiC localization not being affected by the loss of DipM, arguing against a central role of DipM in the control of AmiC activity. On the other hand, our data point to a clear functional link between DipM and SLTs, as DipM shows the same localization pattern as SdpA and SdpB and is required for the recruitment of these proteins to the cell division site. In addition, both DipM (Möll *et al.*, 2010) and the two SLTs require FtsN for midcell localization, suggesting that they are part of the same, FtsN-regulated machinery that mediates invagination of the PG layer during cell constriction (Weiss, 2015). Notably, previous work has revealed a direct interaction between FtsN and DipM (Möll *et al.*, 2010). The positioning of SLTs may thus be achieved by a two-step process in which FtsN first recruits DipM and DipM subsequently mediates the midcell localization of SdpA and SdpB (**Fig. 9**). However, it remains to be clarified whether the localization dependencies observed reflect a direct interaction between DipM and SLTs. Alternatively, DipM may be required to introduce division-specific changes into the structure of PG that then serve as cues for the midcell localization of SdpA and SdpB. Irrespective of the nature of this interplay, the function of DipM must go beyond the stimulation of SLT activity, as indicated by the facts that the Δ*dipM* mutant exhibits more severe defects than the Δ*sdpABC* Δ*pleA* strain and that the combined inactivation of DipM and SLTs produces a synthetic phenotype. Notably, similar observations were made for the relationship between DipM and LdpA-E, demonstrating that the main function of DipM cannot lie in the stimulation of endopeptidase activity either. Collectively, these findings argue for a central regulatory role of DipM that may help to orchestrate the activities of multiple PG hydrolases or, potentially, even synthases during cell constriction in *C. crescentus*.

Aside from DipM, our work has uncovered LdpF as a second non-canonical LytM homolog with a role in *C. crescentus* cell division. Interestingly, the two proteins differ significantly in their domain structure. DipM possesses two tandem LysM motifs with PG binding activity that mediate its recruitment to the cell division site but are dispensable for its function (Goley *et al.*, 2010; Möll *et al.*, 2010; Poggio *et al.*, 2010). LdpF, by contrast, lacks PG-binding domains and instead contains two predicted coiled-coil protein interaction motifs (Lupas, 1996). Its overall architecture is thus very similar to that of EnvC, one of the catalytically inactive LytM factors controlling amidase activity in *E. coli* and *V. cholerae* (Uehara *et al.*, 2009; Uehara *et al.*, 2010; Möll *et al.*, 2014). Our results suggest that LdpF could also be functionally related to EnvC. It likely acts during the late stages of cell division, when AmiC accumulates at the division site, and is required for the proper localization of this predicted amidase to midcell. Moreover, inactivation of LdpF and depletion of AmiC both lead to a lage-stage cell division defect, giving rise to chains of cells that are separated by deep constrictions. Together, these observations indicate that LdpF may interact, directly or indirectly, with AmiC to modulate its putative hydrolytic activity. (**Fig. 9**). The function of EnvC was shown to depend on the association of its coiled-coil regions with the FtsEX complex. Since FtsE and FtsX are conserved in *C. crescentus* and required for efficient cell separation (Goley *et al.*, 2011), a similar mechanism may apply to LdpF. Importantly, however, AmiC is essential for viability in *C. crescentus*, whereas inactivation of LdpF only causes a mild cell division defect. This finding argues against the existence of a simple, linear pathway in which LdpF is the only factor stimulating the activity of AmiC, although it may co-regulate amidase activity by promoting the recruitment of AmiC to midcell. On the other hand, the synthetic phenotype observed for AmiC-depleted Δ*ldpF* cells indicates that AmiC cannot be the only regulatory target of LdpF.

Interestingly, the potential interactors of DipM and LdpF show distinct localization dynamics. SdpA and SdpB relocate to midcell right at the onset of cell division but disperse again shortly before cell fission, suggesting that they contribute specifically to the gradual remodeling of PG during cell constriction. AmiC, on the other hand, is recruited late in the cell cycle and may thus mainly be involved in the final separation of the two daughter cells. Collectively, our results suggest that DipM and LdpF serve as regulatory hubs that coordinate the activities of separate sets of peptidoglyan biosynthetic enzymes at different stages of the division process (**Fig. 9**). The functions of non-canonical LytM homologs in *C. crescentus* thus differ significantly from those in *E. coli*. However, despite the progress made in unraveling the roles of DipM and LdpF, their precise modes of action and regulation still remain to be determined. Solving the underlying molecular mechanisms will enhance our understanding of cell wall biogenesis in bacteria and potentially open new perspectives for the development of antimicrobials directed against the PG hydrolytic machinery.

EXPERIMENTAL PROCEDURES

Bacterial strains and growth conditions

All *C. crescentus* strains used in this study are derived from the synchronizable wild-type strain NA1000 (CB15N) (Evinger and Agabian, 1977; Marks *et al.*, 2010). Cells were grown at 28 °C in peptone-yeast-extract (PYE) medium (Poindexter, 1964). Swarmer cells were isolated by density gradient centrifugation using Percoll (Tsai and Alley, 2001). Plasmids were introduced into *C. crescentus* by electroporation (Ely, 1991). Induction of the *xylX* promoter (Meisenzahl *et al.*, 1997) was achieved by supplementation of the media with 0.3% xylose. Cells carrying inducible fluorescent protein fusions were grown to exponential phase and induced for 3 h prior to microscopic analysis. For *C. crescentus*, antibiotics were used at the following concentrations (µg*ml^{-1}; liquid/solid medium): kanamycin (5/25), gentamicin (0.5/5), spectinomycin (25/50), streptomycin (-/5). *E. coli* TOP10 (Invitrogen) and *E. coli* XL1-Blue (Agilent Technologies) were used for general cloning purposes. Their derivatives were grown aerobically at 37 °C in Luria-Bertani broth (LB) (Carl-Roth, Germany), using antibiotics at the following concentrations (µg*ml^{-1}; liquid/solid medium): ampicillin (200/200), kanamycin (30/50), gentamicin (15/20), spectinomycin (50/100).

Construction of plasmids and bacterial strains

The strains, plasmids, and oligonucleotides used in this study are detailed in **Tables S2-S6**. All plasmid constructs were verified by DNA sequence analysis. Chromosomal in-frame deletions were generated by double-homologous recombination, using a two-step procedure based on the *sacB*-containing suicide vector pNTPS138 (M.R.K. Alley, unpublished) (Thanbichler and Shapiro, 2006). To generate conditional mutants, non-replicating plasmids carrying the genes of interest under the control of the *xylX* promoter (Thanbichler *et al.*, 2007) were integrated at the *xylX* locus. Subsequently, the corresponding endogenous genes were deleted, with xylose added to all media to ensure expression of the complementing, ectopically integrated alleles.

Growth curves

Cultures were grown to exponential phase, with xylose added to the media for conditional mutants. The cells were harvested by centrifugation, washed three times with PYE medium, and resuspended in the same medium to an OD_{600} of 0.01. The suspensions were then transferred to 24-well polystyrene microtiter plates (Becton Dickinson Labware), incubated at 32 °C with double-orbital shaking in an Epoch 2 microplate reader (BioTek, Germany), and analyzed photometrically (OD_{600}) at 15 min intervals.

Spot assays

The strains of interest were grown to exponential phase, with xylose added to the media for conditional mutants. Cells were harvested by centrifugation, washed three times with PYE medium, and resuspended to an OD_{600} of 0.01 in plain PYE medium or PYE medium containing xylose, depending on the target condition. The cultures were then grown for another 6 h, re-adjusted to an OD_{600} of 0.15, and serially diluted in appropriate medium. Finally, aliquots (5 µl) of the suspensions were spotted on solid media, containing additives if appropriate, and incubated for two days prior to imaging.

β-lactamase activity assay

Exponentially growing cultures (1 ml) were mixed with 100 µl nitrocefin solution (1 mg/ml in PBS, prepared from a 10 mg/ml stock solution in DMSO) and incubated with shaking at 28 °C for the indicated period of time. After adjustment to equal cell densities, the suspensions were subjected to spectrophotometric analysis (E_{482}) or transferred to polystyrene microtiter plates for subsequent imaging.

Protein depletion and complementation analysis

To deplete proteins synthesized under the control of the xylose-inducible *xylX* promoter, cells were grown to exponential phase in medium containing 0.3% xylose, harvested by centrifugation for 2 min at 9,000 x g, washed three times, and then resuspended in PYE medium for further analysis. To monitor the depletion of proteins and the resulting phenotypes, samples were taken at regular intervals and analyzed by immunoblotting and DIC microscopy, respectively. Cultures were diluted with fresh medium when necessary to ensure exponential growth throughout the course of the experiments.

Immunoblot analysis

Immunoblot analysis was performed as described previously (Thanbichler and Shapiro, 2006), using rabbit anti-DipM (1:10,000) (Möll *et al.*, 2010) or anti-mCherry (Sigma, Germany) antisera. Goat anti-rabbit immunoglobulin G conjugated to horseradish peroxidase (Perkin Elmer, USA) was used as secondary antibody. Immunocomplexes were detected using the Western Lightning Plus-ECL chemiluminescence reagent (Perkin Elmer, USA). Signals were recorded with a ChemiDoc MP imaging system (Bio-Rad) and analyzed using the Image Lab 5.0 software (Bio-Rad).

Live-cell imaging

To record still images, exponentially growing cells were spotted onto 1% agarose pads. For timelapse imaging, isolated swarmer cells were immobilized on pads made of 1% agarose in PYE medium, and the cover slide was sealed with a 1:1:1 mixture of vaseline, lanolin and paraffin. Images were taken

with an Axio Observer.Z1 (Zeiss) microscope equipped with a Plan Apochromat 100x/1.45 Oil DIC and a Plan Apochromat 100x/1.4 Oil Ph3 phase contrast objective, an ET-mCherry filter set (Chroma, USA), and a pco.edge sCMOS camera (PCO). Images were recorded with VisiView 3.3.0.6 (Visitron Systems, Germany) and processed with Metamorph 7.7.5 (Universal Imaging Group, USA) and Illustrator CS5 (Adobe Systems, USA). To generate demographs, fluorescence intensity profiles were measured with ImageJ 1.47v (http://imagej.nih.gov/ij). The data were then processed in R version 3.1.1 (R Development Core Team, 2012) using the Cell Profiles script (http://github.com/ta-cameron/Cell-Profiles) (Cameron *et al.*, 2014). Cell lengths and width were determined by automated image analysis with Oufti (Paintdakhi *et al.*, 2016). Box and violin plots for the statistical analysis of imaging data were generated in R version 3.3.2 using the boxplotperc (http://github.com/cran/StatDA/blob/master/R/boxplotperc.R) and vioplot2 (http://github.com/mbjoseph/comdis/blob/master/vioplot2.R) scripts, respectively.

Electron cryo-tomography

For electron cryo-microscopy, 2 ml of cell suspension were centrifuged for 5 min at 1,500 x g, and the pellet was resuspended in 30-50 µl of the supernatant. A solution of 10-nm colloidal gold (Ted Pella, USA) was added to the cells immediately before plunge freezing and after treatment with BSA to avoid aggregation of the gold particles (Iancu *et al.*, 2006). A 4-µl droplet of the sample solution was transferred to a glow-discharged R2/2 copper/rhodium grid, then automatically blotted, and plunge-frozen in liquid ethane or a liquid ethane/propane mixture (Tivol *et al.*, 2008) using a Vitrobot (FEI Company, USA). The grids were stored under liquid nitrogen until data collection. Images were acquired using the FEI Polara TM (FEI Company, USA) 300 kV FEG transmission electron microscope, equipped with a Gatan energy filter (slit width 20 eV) on a lens-coupled, cooled 4k x 4k Ultracam (Gatan, USA). The pixel size on the specimen plane was 0.961 nm. Single-axis tilt series were recorded from -60 ° to 60 ° with an increment of 1 ° and an underfocus of 12 µm, using Leginon (Suloway *et al.*, 2009). The cumulative dose was limited to 200 e/A2. Three-dimensional reconstructions were obtained using the IMOD software package (Mastronarde and Held, 2017).

Bioinformatic analysis

Protein sequences containing LytM (Peptidase_M23; PF01551) or SLT (SLT; PF01464) domains were retrieved from the UniProt Knowledgebase (The UniProt Consortium, 2017). Their overall domain composition was determined using the SMART server (Letunic *et al.*, 2015). The prediction of protein localization and membrane topology was performed with Signal-BLAST (Frank and Sippl, 2008) and TMHMM (Krogh *et al.*, 2001), respectively.

ACKNOWLEDGEMENTS

We thank Stephanie Steede and Julia Rosum for excellent technical assistance, Patrick Viollier for providing plasmids, and Erin Goley for sharing data on *C. crescentus* FtsEX before publication. Moreover, we are grateful to Daniela Kiekebusch and Muriel van Teeseling for critical reading of the manuscript. This work was funded by core support from Philipps-Universität Marburg (to MT), a Max Planck Fellowship from the Max Planck Society (to MT), and funds from the Howard Hughes Medical Institute (to GJJ). AIM acknowledges funding from the International Max Planck Research School for Environmental, Cellular and Molecular Microbiology (IMPRS-Mic).

AUTHOR CONTRIBUTIONS

AZ, MB, AM, and KK performed all genetic and cell biological analyses. AIM contributed to the phenotypic characterization of mutant strains. AB and GJJ conducted the electron cryo-tomography studies. AZ, AM, and MT designed the study. AM, MB, and MT wrote the manuscript.

CONFLICT OF INTEREST STATEMENT

The authors have no conflicts of interest related to this work.

REFERENCES

Aaron, M., Charbon, G., Lam, H., Schwarz, H., Vollmer, W., and Jacobs-Wagner, C. (2007) The tubulin homologue FtsZ contributes to cell elongation by guiding cell wall precursor synthesis in *Caulobacter crescentus*. *Mol Microbiol* **64**: 938-952.

Alcorlo, M., Martinez-Caballero, S., Molina, R., and Hermoso, J.A. (2017) Carbohydrate recognition and lysis by bacterial peptidoglycan hydrolases. *Curr Opin Struct Biol* **44**: 87-100.

Alyahya, S.A., Alexander, R., Costa, T., Henriques, A.O., Emonet, T., and Jacobs-Wagner, C. (2009) RodZ, a component of the bacterial core morphogenic apparatus. *Proc Natl Acad Sci U S A* **106**: 1239-1244.

Bochtler, M., Odintsov, S.G., Marcyjaniak, M., and Sabala, I. (2004) Similar active sites in lysostaphins and D-Ala-D-Ala metallopeptidases. *Protein Sci* **13**: 854-861.

Brown, P.J., Hardy, G.G., Trimble, M.J., and Brun, Y.V. (2009) Complex regulatory pathways coordinate cell-cycle progression and development in *Caulobacter crescentus*. *Adv Microb Physiol* **54**: 1-101.

Cameron, T.A., Anderson-Furgeson, J., Zupan, J.R., Zik, J.J., and Zambryski, P.C. (2014) Peptidoglycan synthesis machinery in *Agrobacterium tumefaciens* during unipolar growth and cell division. *MBio* **5**: e01219-01214.

Cho, H., Uehara, T., and Bernhardt, T.G. (2014) Beta-lactam antibiotics induce a lethal malfunctioning of the bacterial cell wall synthesis machinery. *Cell* **159**: 1300-1311.

Christen, B., Abeliuk, E., Collier, J.M., Kalogeraki, V.S., Passarelli, B., Coller, J.A., Fero, M.J., McAdams, H.H., and Shapiro, L. (2011) The essential genome of a bacterium. *Mol Syst Biol* **7**: 528.

Costa, T., Priyadarshini, R., and Jacobs-Wagner, C. (2008) Localization of PBP3 in *Caulobacter crescentus* is highly dynamic and largely relies on its functional transpeptidase domain. *Mol Microbiol* **70**: 634-651.

den Blaauwen, T., de Pedro, M.A., Nguyen-Disteche, M., and Ayala, J.A. (2008) Morphogenesis of rod-shaped sacculi. *FEMS Microbiol Rev* **32**: 321-344.

Dominguez-Gil, T., Molina, R., Alcorlo, M., and Hermoso, J.A. (2016) Renew or die: The molecular mechanisms of peptidoglycan recycling and antibiotic resistance in Gram-negative pathogens. *Drug Resist Updat* **28**: 91-104.

Dye, N.A., Pincus, Z., Theriot, J.A., Shapiro, L., and Gitai, Z. (2005) Two independent spiral structures control cell shape in *Caulobacter*. *Proc Natl Acad Sci U S A* **102**: 18608-18613.

Ely, B. (1991) Genetics of *Caulobacter crescentus*. *Methods Enzymol* **204**: 372-384.

Evinger, M., and Agabian, N. (1977) Envelope-associated nucleoid from *Caulobacter crescentus* stalked and swarmer cells. *J Bacteriol* **132**: 294-301.

Figge, R.M., Divakaruni, A.V., and Gober, J.W. (2004) MreB, the cell shape-determining bacterial actin homologue, co-ordinates cell wall morphogenesis in *Caulobacter crescentus*. *Mol Microbiol* **51**: 1321-1332.

Frank, K., and Sippl, M.J. (2008) High-performance signal peptide prediction based on sequence alignment techniques. *Bioinformatics* **24**: 2172-2176.

Gerding, M.A., Ogata, Y., Pecora, N.D., Niki, H., and de Boer, P.A. (2007) The trans-envelope Tol-Pal complex is part of the cell division machinery and required for proper outer-membrane invagination during cell constriction in *E. coli*. *Mol Microbiol* **63**: 1008-1025.

Gitai, Z., Dye, N., and Shapiro, L. (2004) An actin-like gene can determine cell polarity in bacteria. *Proc Natl Acad Sci U S A* **101**: 8643-8648.

Goley, E.D., Comolli, L.R., Fero, K.E., Downing, K.H., and Shapiro, L. (2010) DipM links peptidoglycan remodelling to outer membrane organization in *Caulobacter*. *Mol Microbiol* **77**: 56-73.

Goley, E.D., Yeh, Y.C., Hong, S.H., Fero, M.J., Abeliuk, E., McAdams, H.H., and Shapiro, L. (2011) Assembly of the *Caulobacter* cell division machine. *Mol Microbiol* **80**: 1680-1698.

Heidrich, C., Templin, M.F., Ursinus, A., Merdanovic, M., Berger, J., Schwarz, H., de Pedro, M.A., and Höltje, J.V. (2001) Involvement of N-acetylmuramyl-L-alanine amidases in cell separation and antibiotic-induced autolysis of *Escherichia coli*. *Mol Microbiol* **41**: 167-178.

Heidrich, C., Ursinus, A., Berger, J., Schwarz, H., and Höltje, J.V. (2002) Effects of multiple deletions of murein hydrolases on viability, septum cleavage, and sensitivity to large toxic molecules in *Escherichia coli*. *J Bacteriol* **184**: 6093-6099.

Hocking, J., Priyadarshini, R., Takacs, C.N., Costa, T., Dye, N.A., Shapiro, L., Vollmer, W., and Jacobs-Wagner, C. (2012) Osmolality-dependent relocation of penicillin-binding protein PBP2 to the division site in *Caulobacter crescentus*. *J Bacteriol* **194**: 3116-3127.

Höltje, J.V. (1998) Growth of the stress-bearing and shape-maintaining murein sacculus of *Escherichia coli*. *Microbiol Mol Biol Rev* **62**: 181-203.

Huitema, E., Pritchard, S., Matteson, D., Radhakrishnan, S.K., and Viollier, P.H. (2006) Bacterial birth scar proteins mark future flagellum assembly site. *Cell* **124**: 1025-1037.

Iancu, C.V., Tivol, W.F., Schooler, J.B., Dias, D.P., Henderson, G.P., Murphy, G.E., Wright, E.R., Li, Z., Yu, Z., Briegel, A., Gan, L., He, Y., and Jensen, G.J. (2006) Electron cryotomography sample preparation using the Vitrobot. *Nat Protoc* **1**: 2813-2819.

Jacobs, C., Huang, L.J., Bartowsky, E., Normark, S., and Park, J.T. (1994) Bacterial cell wall recycling provides cytosolic muropeptides as effectors for beta-lactamase induction. *EMBO J* **13**: 4684-4694.

Korsak, D., Liebscher, S., and Vollmer, W. (2005) Susceptibility to antibiotics and beta-lactamase induction in murein hydrolase mutants of *Escherichia coli*. *Antimicrob Agents Chemother* **49**: 1404-1409.

Krogh, A., Larsson, B., von Heijne, G., and Sonnhammer, E.L. (2001) Predicting transmembrane protein topology with a hidden Markov model: application to complete genomes. *J Mol Biol* **305**: 567-580.

Kühn, J., Briegel, A., Mörschel, E., Kahnt, J., Leser, K., Wick, S., Jensen, G.J., and Thanbichler, M. (2010) Bactofilins, a ubiquitous class of cytoskeletal proteins mediating polar localization of a cell wall synthase in *Caulobacter crescentus*. *EMBO J* **29**: 327-339.

Letunic, I., Doerks, T., and Bork, P. (2015) SMART: recent updates, new developments and status in 2015. *Nucleic Acids Res* **43**: D257-260.

Lupas, A. (1996) Coiled coils: new structures and new functions. *Trends Biochem Sci* **21**: 375-382.

Marks, M.E., Castro-Rojas, C.M., Teiling, C., Du, L., Kapatral, V., Walunas, T.L., and Crosson, S. (2010) The genetic basis of laboratory adaptation in *Caulobacter crescentus*. *J Bacteriol* **192**: 3678-3688.

Mastronarde, D.N., and Held, S.R. (2017) Automated tilt series alignment and tomographic reconstruction in IMOD. *J Struct Biol* **197**: 102-113.

Mavrici, D., Marakalala, M.J., Holton, J.M., Prigozhin, D.M., Gee, C.L., Zhang, Y.J., Rubin, E.J., and Alber, T. (2014) *Mycobacterium tuberculosis* FtsX extracellular domain activates the peptidoglycan hydrolase, RipC. *Proc Natl Acad Sci U S A* **111**: 8037-8042.

Meisenzahl, A.C., Shapiro, L., and Jenal, U. (1997) Isolation and characterization of a xylose-dependent promoter from *Caulobacter crescentus*. *J Bacteriol* **179**: 592-600.

Meisner, J., Montero Llopis, P., Sham, L.T., Garner, E., Bernhardt, T.G., and Rudner, D.Z. (2013) FtsEX is required for CwlO peptidoglycan hydrolase activity during cell wall elongation in *Bacillus subtilis*. *Mol Microbiol* **89**: 1069-1083.

Möll, A., Dörr, T., Alvarez, L., Chao, M.C., Davis, B.M., Cava, F., and Waldor, M.K. (2014) Cell separation in *Vibrio cholerae* is mediated by a single amidase whose action is modulated by two nonredundant activators. *J Bacteriol* **196**: 3937-3948.

Möll, A., Schlimpert, S., Briegel, A., Jensen, G.J., and Thanbichler, M. (2010) DipM, a new factor required for peptidoglycan remodelling during cell division in *Caulobacter crescentus*. *Mol Microbiol* **77**: 90-107.

Möll, A., and Thanbichler, M. (2009) FtsN-like proteins are conserved components of the cell division machinery in proteobacteria. *Mol Microbiol* **72**: 1037-1053.

Nelson, D.E., and Young, K.D. (2000) Penicillin binding protein 5 affects cell diameter, contour, and morphology of *Escherichia coli*. *J Bacteriol* **182**: 1714-1721.

Paintdakhi, A., Parry, B., Campos, M., Irnov, I., Elf, J., Surovtsev, I., and Jacobs-Wagner, C. (2016) Oufti: an integrated software package for high-accuracy, high-throughput quantitative microscopy analysis. *Mol Microbiol* **99**: 767-777.

Palmer, T., and Berks, B.C. (2012) The twin-arginine translocation (Tat) protein export pathway. *Nat Rev Microbiol* **10**: 483-496.

Peters, K., Kannan, S., Rao, V.A., Biboy, J., Vollmer, D., Erickson, S.W., Lewis, R.J., Young, K.D., and Vollmer, W. (2016) The redundancy of peptidoglycan carboxypeptidases ensures robust cell shape maintenance in *Escherichia coli*. *MBio* **7**.

Peters, N.T., Morlot, C., Yang, D.C., Uehara, T., Vernet, T., and Bernhardt, T.G. (2013) Structure-function analysis of the LytM domain of EnvC, an activator of cell wall remodelling at the *Escherichia coli* division site. *Mol Microbiol* **89**: 690-701.

Poggio, S., Takacs, C.N., Vollmer, W., and Jacobs-Wagner, C. (2010) A protein critical for cell constriction in the Gram-negative bacterium *Caulobacter crescentus* localizes at the division site through its peptidoglycan-binding LysM domains. *Mol Microbiol* **77**: 74-89.

Poindexter, J.S. (1964) Biological properties and classification of the *Caulobacter* group. *Bacteriol Rev* **28**: 231-295.

Priyadarshini, R., de Pedro, M.A., and Young, K.D. (2007) Role of peptidoglycan amidases in the development and morphology of the division septum in *Escherichia coli*. *J Bacteriol* **189**: 5334-5347.

Priyadarshini, R., Popham, D.L., and Young, K.D. (2006) Daughter cell separation by penicillin-binding proteins and peptidoglycan amidases in *Escherichia coli*. *J Bacteriol* **188**: 5345-5355.

R Development Core Team (2012) *R: a language and environment for statistical computing*. The R Foundation for Statistical Computing, Vienna, Austria.

Randich, A.M., and Brun, Y.V. (2015) Molecular mechanisms for the evolution of bacterial morphologies and growth modes. *Front Microbiol* **6**: 580.

Rice, K.C., and Bayles, K.W. (2008) Molecular control of bacterial death and lysis. *Microbiol Mol Biol Rev* **72**: 85-109, table of contents.

Sham, L.T., Jensen, K.R., Bruce, K.E., and Winkler, M.E. (2013) Involvement of FtsE ATPase and FtsX extracellular loops 1 and 2 in FtsEX-PcsB complex function in cell division of *Streptococcus pneumoniae* D39. *MBio* **4**: e00431-13.

Simm, A.M., Higgins, C.S., Pullan, S.T., Avison, M.B., Niumsup, P., Erdozain, O., Bennett, P.M., and Walsh, T.R. (2001) A novel metallo-beta-lactamase, Mbl1b, produced by the environmental bacterium *Caulobacter crescentus*. *FEBS Lett* **509**: 350-354.

Stapleton, M.R., Horsburgh, M.J., Hayhurst, E.J., Wright, L., Jonsson, I.M., Tarkowski, A., Kokai-Kun, J.F., Mond, J.J., and Foster, S.J. (2007) Characterization of IsaA and SceD, two putative lytic transglycosylases of *Staphylococcus aureus*. *J Bacteriol* **189**: 7316-7325.

Stohl, E.A., Lenz, J.D., Dillard, J.P., and Seifert, H.S. (2015) The gonococcal NlpD protein facilitates cell separation by activating peptidoglycan cleavage by AmiC. *J Bacteriol* **198**: 615-622.

Strobel, W., Möll, A., Kiekebusch, D., Klein, K.E., and Thanbichler, M. (2014) Function and localization dynamics of bifunctional penicillin-binding proteins in *Caulobacter crescentus*. *J Bacteriol* **196**: 1627-1639.

Suloway, C., Shi, J., Cheng, A., Pulokas, J., Carragher, B., Potter, C.S., Zheng, S.Q., Agard, D.A., and Jensen, G.J. (2009) Fully automated, sequential tilt-series acquisition with Leginon. *J Struct Biol* **167**: 11-18.

Takacs, C.N., Poggio, S., Charbon, G., Pucheault, M., Vollmer, W., and Jacobs-Wagner, C. (2010) MreB drives de novo rod morphogenesis in *Caulobacter crescentus* via remodeling of the cell wall. *J Bacteriol* **192**: 1671-1684.

Thanbichler, M., Iniesta, A.A., and Shapiro, L. (2007) A comprehensive set of plasmids for vanillate- and xylose-inducible gene expression in *Caulobacter crescentus*. *Nucleic Acids Res* **35**: e137.

Thanbichler, M., and Shapiro, L. (2006) MipZ, a spatial regulator coordinating chromosome segregation with cell division in *Caulobacter*. *Cell* **126**: 147-162.

The UniProt Consortium (2017) UniProt: the universal protein knowledgebase. *Nucleic Acids Res* **45**: D158-D169.

Tivol, W.F., Briegel, A., and Jensen, G.J. (2008) An improved cryogen for plunge freezing. *Microsc Microanal* **14**: 375-379.

Tsai, J.W., and Alley, M.R. (2001) Proteolysis of the *Caulobacter* McpA chemoreceptor is cell cycle regulated by a ClpX-dependent pathway. *J Bacteriol* **183**: 5001-5007.

Typas, A., Banzhaf, M., Gross, C.A., and Vollmer, W. (2012) From the regulation of peptidoglycan synthesis to bacterial growth and morphology. *Nat Rev Microbiol* **10**: 123-136.

Uehara, T., and Bernhardt, T.G. (2011) More than just lysins: peptidoglycan hydrolases tailor the cell wall. *Curr Opin Microbiol* **14**: 698-703.

Uehara, T., Dinh, T., and Bernhardt, T.G. (2009) LytM-domain factors are required for daughter cell separation and rapid ampicillin-induced lysis in *Escherichia coli*. *J Bacteriol* **191**: 5094-5107.

Uehara, T., Parzych, K.R., Dinh, T., and Bernhardt, T.G. (2010) Daughter cell separation is controlled by cytokinetic ring-activated cell wall hydrolysis. *EMBO J* **29**: 1412-1422.

van Heijenoort, J. (2011) Peptidoglycan hydrolases of *Escherichia coli*. *Microbiol Mol Biol Rev* **75**: 636-663.

Viollier, P.H., and Shapiro, L. (2003) A lytic transglycosylase homologue, PleA, is required for the assembly of pili and the flagellum at the *Caulobacter crescentus* cell pole. *Mol Microbiol* **49**: 331-345.

Vollmer, W., Joris, B., Charlier, P., and Foster, S. (2008) Bacterial peptidoglycan (murein) hydrolases. *FEMS Microbiol Rev* **32**: 259-286.

Weiss, D.S. (2015) Last but not least: new insights into how FtsN triggers constriction during *Escherichia coli* cell division. *Mol Microbiol* **95**: 903-909.

West, L., Yang, D., and Stephens, C. (2002) Use of the *Caulobacter crescentus* genome sequence to develop a method for systematic genetic mapping. *J Bacteriol* **184**: 2155-2166.

Yakhnina, A.A., and Gitai, Z. (2013) Diverse functions for six glycosyltransferases in *Caulobacter* crescentus cell wall assembly. *J Bacteriol* **195**: 4527-4535.

Yakhnina, A.A., McManus, H.R., and Bernhardt, T.G. (2015) The cell wall amidase AmiB is essential for *Pseudomonas aeruginosa* cell division, drug resistance and viability. *Mol Microbiol* **97**: 957-973.

Yang, D.C., Peters, N.T., Parzych, K.R., Uehara, T., Markovski, M., and Bernhardt, T.G. (2011) An ATP-binding cassette transporter-like complex governs cell-wall hydrolysis at the bacterial cytokinetic ring. *Proc Natl Acad Sci U S A* **108**: E1052-1060.

Yang, D.C., Tan, K., Joachimiak, A., and Bernhardt, T.G. (2012) A conformational switch controls cell wall-remodelling enzymes required for bacterial cell division. *Mol Microbiol* **85**: 768-781.

Yeh, Y.C., Comolli, L.R., Downing, K.H., Shapiro, L., and McAdams, H.H. (2010) The *Caulobacter* Tol-Pal complex is essential for outer membrane integrity and the positioning of a polar localization factor. *J Bacteriol* **192**: 4847-4858.

Zeng, X., and Lin, J. (2013) Beta-lactamase induction and cell wall metabolism in Gram-negative bacteria. *Front Microbiol* **4**: 128.

FIGURE LEGENDS

Figure 1. Role of LytM homologs. (A) Schematic representation of the seven LytM homologs encoded in the *C. crescentus* genome. Domains are indicated in color. Proteins predicted to be catalytically inactive are highlighted in red. The corresponding ORF numbers are given in **Table S1**. **(B)** Morphology of strains lacking one or multiple LytM factors. Cells of strains NA1000 (WT), MT258 (Δ*dipM*), AM438 (Δ*ldpABCDE*), AM369 (Δ*ldpF*), and AZ52 (Δ*ldpABCDEF*) were grown to exponential phase and analyzed by DIC microscopy (bar: 3 µm). **(C)** Distribution of cell lengths and widths in populations of LytM factor-deficient cells. Micrographs of the strains described in (B) were subjected to automated image analysis. The values obtained (n = 312 per strain) are shown as box plots, with the thick line indicating the median, the box the interquartile range, and the wiskers the 2nd and 98th percentile. In addition, rotated kernel density plots (orange) are given for each dataset to indicate the distribution of the data (*** $p < 10^{-6}$; t-test). **(D)** Ultrastructural changes induced by the lack of LdpF. Strain AM369 (Δ*ldpF*) was grown to exponential phase and analyzed by cryo-electron tomography. Shown are virtual sections through the division plane of chained cells (bars: 100 nm). IM, inner membrane, PG, peptidoglycan layer. OM, outer membrane. SL, surface layer. **(E)** Salt sensitivity of strains lacking LytM factors. Cultures of strains NA1000 (WT), MT258 (Δ*dipM*), AM365 (Δ*ldpB*), AM369 (Δ*ldpF*), AZ91 (Δ*ldpBF*), AM438 (Δ*ldpABCDE*), and AZ52 (Δ*ldpABCDEF*) were serially diluted, spotted on solid medium containing no or 0.3% NaCl, and analyzed after two days of incubation. **(F)** Salt-induced morphological changes of LdpF-deficient cells. Strains NA1000 (WT) and AM369 (Δ*ldpF*) were grown to early exponential phase and exposed to 0.3% NaCl. Samples were taken immediately before (0 min) and at the indicated time points after supplementation of the media and analyzed by DIC microscopy (bar: 3 µm). **(G)** Impaired division of Δ*ldpF* cells in high-salt conditions. Cells treated as described in (F) were analyzed for their lengths before and after addition of 0.3% NaCl. The data are shown as box plots, with the whiskers including all data points within 1.5*IQR (n = 212 per time point and strain). At t = 165 min (+ NaCl), the Δ*ldpF* population included 69% elongated doublets (> 4.2 µm) and 11% cell chains with more than two compartments (compare **Fig. S1D**). **(H)** Growth of the Δ*ldpF* mutant at elevated salt concentrations. The density of the cultures (OD_{600}) described in (F) was determined at regular intervals by photometric (+ NaCl) measurements. The time point at which salt (0.3%) was added to the media is marked by an arrow. Cultures not exposed to NaCl were analyzed as controls (- NaCl).

Figure 2. Essentiality of DipM in strains lacking multiple LytM factors. (A) Decreased viability of LytM factor-deficient cells after depletion of DipM. Strains NA1000 (WT), AM369 (Δ*ldpF*), AM438 (Δ*ldpABCDE*), AZ52 (Δ*ldpABCDEF*), MAB360 (Δ*dipM* P_{xyl}::P_{xyl}-*dipM*), KK31 (Δ*ldpF* Δ*dipM* P_{xyl}::P_{xyl}-*dipM*), KK37 (Δ*ldpABCDEF* Δ*dipM* P_{xyl}::P_{xyl}-*dipM*), and KK38 (Δ*ldpABCDE* Δ*dipM* P_{xyl}::P_{xyl}-*dipM*) were grown to

exponential phase, with xylose added to the media for conditional mutants. The cultures were serially diluted, spotted on medium containing (PYE + xylose) or lacking (PYE) inducer, and incubated for two days prior to imaging. **(B)** Effect of DipM depletion on the growth of LytM factor-deficient cells. The DipM-containing (+ DipM) strains AM369 (Δ*ldpF*), AM438 (Δ*ldpABCDE*), AZ52 (Δ*ldpABCDEF*) and the corresponding conditional *dipM* mutants (- DipM) KK31 (Δ*ldpF* Δ*dipM* P_{xyl}::P_{xyl}-*dipM*), KK37 (Δ*ldpABCDEF* Δ*dipM* P_{xyl}::P_{xyl}-*dipM*), and KK38 (Δ*ldpABCDE* Δ*dipM* P_{xyl}::P_{xyl}-*dipM*) were grown to exponential phase, with xylose added to the media for the three conditional mutants. After washing, the cells were resuspended in medium lacking inducer, and their growth was followed in a microplate reader. **(C)** Cell morphology after depletion of DipM in the WT (MAB360), Δ*ldpF* (KK31), Δ*ldpABCDE* (KK38), and Δ*ldpABCDEF* (KK37) backgrounds. The indicated strains were grown to exponential phase in xylose-containing medium, washed, and then cultivated for 12 h in medium containing (+ xylose) or lacking (- xylose) inducer prior to imaging by DIC microscopy (bar: 3 µm). **(D)** Distribution of cell lengths and widths in populations of LytM factor-deficient strains under conditions of DipM depletion. Micrographs of the strains described in (C) were subjected to automated image analysis. The data obtained (n > 311) are shown as box plots and rotated kernel density plots, as defined in **Fig. 1C** (*** $p < 10^{-6}$; t-test). The median (purple) and interquartile range (light purple) of the lengths and widths of NA1000 wild-type cells are given as a reference (taken from Figure 1C).

Figure 3. Role of soluble lytic transglycosylases. (A) Schematic representation of the four SLT homologs encoded in the *C. crescentus* genome. Domains are indicated in color. The corresponding ORF numbers are given in **Table S1**. **(B)** Morphology of strains lacking one or multiple SLTs. Cells of strains NA1000 (WT), AM440 (Δ*sdpABC*), and AZ93 (Δ*sdpABC* Δ*pleA*) were grown to exponential phase and analyzed by DIC microscopy (bar: 3 µm). **(C)** Distribution of cell lengths and widths in populations of SLT-deficient strains. Micrographs of the strains described in (B) were subjected to automated image analysis. The data obtained (n = 503 per strain) are shown as box plots and rotated kernel density plots, as defined in **Fig. 1C** (*** $p < 10^{-6}$; t-test). **(D)** Viability of SLT-deficient cells. Exponentially growing cultures of strains NA1000 (WT), AM440 (Δ*sdpABC*), and AZ93 (Δ*sdpABC* Δ*pleA*) were serially diluted, spotted on solid medium, and incubated for two days prior to imaging. **(E)** Formation of outer membrane blebs by SdpABC-deficient cells. Strains NA1000 (WT) and AM440 (Δ*sdpABC*) were transformed with plasmid pEJ216 (P_{xyl}-*torA'-tdimer2*) and induced for 2 h with 0.3% xylose prior to analysis by DIC and fluorescence microscopy (bar: 3 µm). Outer membrane blebs are indicated by arrowheads. **(F)** Ultrastructure of SLT-deficient cells. Strain AM440 (Δ*sdpABC*) was grown to exponential phase and analyzed by cryo-electron tomography. Shown are virtual sections through the polar regions and the division plane (bars: 200 nm). IM, inner membrane, PG, peptidoglycan layer. OM, outer membrane. SL, surface layer.

Figure 4. Requirement of SdpA and DipM for ampicillin resistance. (A) Ampicillin sensitivity of PG hydrolase mutants. Cultures of strains NA1000 (WT), MT258 (Δ*dipM*), AM440 (Δ*sdpABC*), and AZ52 (Δ*ldpABCDEF*) were serially diluted, spotted in parallel on plain PYE medium and PYE medium containing 50 µg/ml ampicillin, and incubated for two days prior to imaging. **(B)** Ampicillin sensitivity of cells lacking one or more SLT genes. Cultures of strains NA1000 (WT) and CS606 (Δ*bla*) were analyzed as described in (A). **(C)** β-lactamase activity of PG hydrolase mutants. The strains described in (A) and the control strain CS606 (Δ*bla*) were grown to exponential phase in the presence (+ amp) or absence (- amp) of 10 µg/ml ampicillin and incubated for 60 min with the chromogenic β-lactam nitrocefin. The hydrolysis of nitrocefin is evidenced by the formation of a red-colored product. A reaction lacking cells served as a control. **(D)** Requirement of SdpA for proper cell division in the presence of ampicillin. Cells of strains NA1000 (WT) and AM399 (Δ*sdpA*) were grown to exponential phase and exposed to 10 µg/ml ampicillin. Samples were taken immediately before (0 min) and at the indicated time points after supplementation of the media and analyzed by DIC microscopy (bar: 3 µm). **(E)** Distribution of cell lengths in the cultures analyzed in (D). The data are shown as box plots, with the whiskers including all data points within 1.5*IQR (n = 215 per time point and strain).

Figure 5. Dynamic subcellular localization of SdpA, SdpB and AmiC. (A-C) Localization of SdpA, SdpB, and AmiC over the course of the cell cycle. Strains AM480 (P_{xyl}::P_{xyl}-*sdpA-mCherry*), AZ127 (P_{xyl}::P_{xyl}-*sdpB-mCherry*), and MT248 (P_{xyl}::P_{xyl}-*amiC-mCherry*) were grown to exponential phase and imaged by DIC and fluorescence microscopy. Shown are cells from the mixed cultures arranged according to their developmental state. **(D)** Position of SdpA, SdpB and AmiC in the hierarchy of the divisome assembly. Swarmer cells of strains MT196 (P_{xyl}::P_{xyl}-*ftsZ-eyfp*), AM480 (P_{xyl}::P_{xyl}-*sdpA-mCherry*), MT46 (AM480 (P_{xyl}::P_{xyl}-*ftsN-egfp*), AZ127 (P_{xyl}::P_{xyl}-*sdpB-mCherry*), MT248 (P_{xyl}::P_{xyl}-*amiC-mCherry*), and NR1371 (Δ*bla* P_{xyl}::P_{xyl}-*tipN-egfp*) were transferred into PYE medium and followed for the duration of one cell cycle. Samples were taken at regular intervals and analyzed for the fraction of cells showing a noticeable focus of the indicated protein at midcell (n > 300 for each time point and strain).

Figure 6. Role of non-canonical LytM factors in SLT and amidase localization. (A) Localization pattern of SdpA-mCherry in wild-type and Δ*dipM* cells. After synchronization, cells of strains AM480 (P_{xyl}::P_{xyl}-*sdpA-mCherry*) and MAB203 (Δ*dipM* P_{xyl}::P_{xyl}-*sdpA-mCherry*) were cultivated until they reached the late pre-divisional stage and analyzed by DIC and fluorescence microscopy. Shown are representative images (bars: 3 µm) and demographs giving the distribution of fluorescence in a random subpopulation of cells (n = 200 per strain). To generate the graphs, fluorescence profiles were measured and stacked on top of each other according to cell length. **(B)** Localization pattern of SdpB-mCherry in wild-type and Δ*dipM* cells. The analysis was performed as described in (A), using strains AZ127 (P_{xyl}::P_{xyl}-*sdpB-mCherry*) and MAB308 (Δ*dipM* P_{xyl}::P_{xyl}-*sdpB-mCherry*). **(C)** Localization

pattern of AmiC-mCherry in wild-type and Δ*ldpF* cells. The analysis was performed as described in (A), using strains MT248 (P_{xyl}::P_{xyl}-*amiC-mCherry*) and AZ181 (Δ*ldpF* P_{xyl}::P_{xyl}-*amiC-mCherry*).

Figure 7. Synthetic effects of LdpF and AmiC deficiency. (A) Reduced viability of LdpF-deficient cells upon reduced expression of *amiC*. Strains NA1000 (WT), AM369 (Δ*ldpF*), MAB386 (Δ*amiC* P_{xyl}::P_{xyl}-*amiC*), and MAB384 (Δ*ldpF* Δ*amiC* P_{xyl}::P_{xyl}-*amiC*) were grown to exponential phase, with xylose added to the media for conditional mutants. The cultures were serially diluted, spotted on medium containing (PYE + xylose) or lacking (PYE) inducer, and incubated for two days prior to imaging. **(B)** Effect of reduced AmiC levels on the growth of LdpF-deficient cells. Strains AM369 (Δ*ldpF*) (+ AmiC) and MAB384 (Δ*ldpF* Δ*amiC* P_{xyl}::P_{xyl}-*amiC*) (- AmiC) were grown to exponential phase, with xylose added to the media for the conditional mutant. After washing, the cells were resuspended in medium lacking inducer, and their growth was followed in a microplate reader. Strain MAB386 (Δ*amiC* P_{xyl}::P_{xyl}-*amiC*) (- AmiC *ldpF*$^{+}$) was analyzed as a control. **(C)** Cell morphology after reduced expression of *amiC* in the WT (MAB386) and Δ*ldpF* (MAB384) backgrounds. The two strains were grown to exponential phase in xylose-containing medium, washed, and then cultivated for 12 h in medium containing (+ xylose) or lacking (- xylose) inducer prior to imaging by DIC microscopy (bar: 3 µm). Arrowheads point to long tubular connections between cells. **(D)** Distribution of cell lengths and widths in populations of Δ*ldpF* cells after reduction of the AmiC levels. Micrographs of the strains described in (C) were subjected to automated image analysis. The data obtained (n = 327 per strain) are shown as box plots and rotated kernel density plots, as defined in **Fig. 1C** (*** $p < 10^{-6}$; t-test).

Figure 8. Essentiality of DipM in strains lacking multiple SLTs. (A) Decreased viability of SLT-deficient cells after depletion of DipM. Strains NA1000 (WT), AM440 (Δ*sdpABC*), AZ93 (Δ*sdpABC* Δ*pleA*), MAB360 (Δ*dipM* P_{xyl}::P_{xyl}-*dipM*), KK39 (Δ*sdpABC* Δ*pleA* Δ*dipM* P_{xyl}::P_{xyl}-*dipM*), and KK46 (Δ*sdpABC* Δ*dipM* P_{xyl}::P_{xyl}-*dipM*) were grown to exponential phase, with xylose added to the media for conditional mutants. The cultures were serially diluted, spotted on medium containing (PYE + xylose) or lacking (PYE) inducer, and incubated for two days prior to imaging. **(B)** Effect of DipM depletion on the growth of SLT-deficient cells. The DipM-containing (+ DipM) strains AM440 (Δ*sdpABC*), AZ93 (Δ*sdpABC* Δ*pleA*) and the conditional *dipM* (- DipM) mutants KK46 (Δ*sdpABC* Δ*dipM* P_{xyl}::P_{xyl}-*dipM*) and KK39 (Δ*sdpABC* Δ*pleA* Δ*dipM* P_{xyl}::P_{xyl}-*dipM*) were grown to exponential phase, with xylose added to the media for the two conditional mutants. After washing, the cells were resuspended in medium lacking inducer, and their growth was followed in a microplate reader. Strain MAB360 (Δ*dipM* P_{xyl}::P_{xyl}-*dipM*) (- DipM SLT^{+}) was analyzed in parallel as a control. **(C)** Cell morphology after depletion of DipM in the WT (MAB360), Δ*sdpABC* (KK46), and Δ*sdpABC* Δ*pleA* (KK39) backgrounds. The indicated strains were grown to exponential phase in xylose-containing medium, washed, and then cultivated for 12 h in medium containing (+ xylose) or lacking (- xylose) inducer prior to imaging by

DIC microscopy (bar: 3 µm). Arrowheads indicate membrane blebs. **(D)** Distribution of cell lengths and widths in populations of SLT-deficient strains after DipM depletion. Micrographs of the strains described in (C) were subjected to automated image analysis. The data obtained (n = 503 per strain) are shown as box plots and rotated kernel density plots, as defined in **Fig. 1C** (*** $p < 10^{-6}$; t-test).

Figure 9. Model for the roles of DipM and LdpF in the regulation of PG biosynthesis. The non-canonical LytM factors DipM and LdpF may act as regulatory hubs that help coordinate the activity of PG remodeling enzymes at subsequent stages of the division cycle. LysM domains are shown in green, LytM domains in purple, SLT domains in red, and amidase domains in blue. Suggested, direct or indirect interactions are indicated by double-headed arrows. Putative, thus-far unknown interaction partners are labeled with question marks. IM, inner membrane. PG, peptidoglycan.

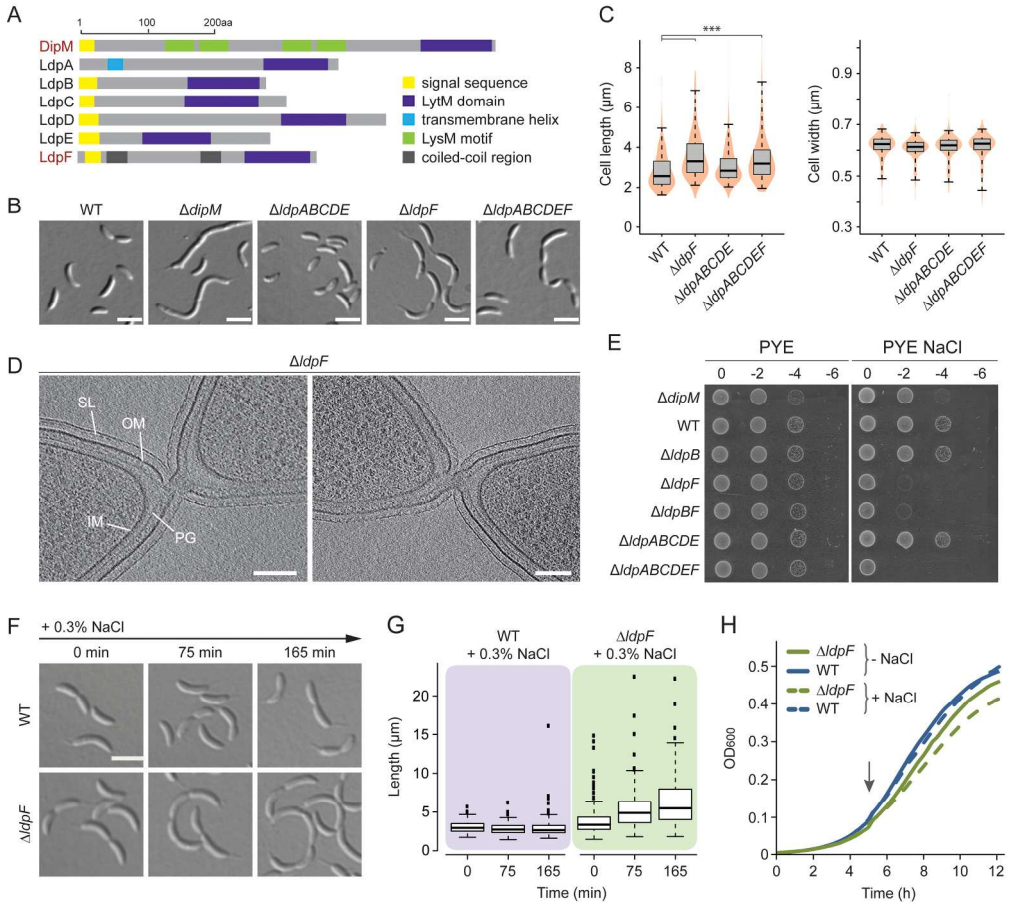

216x194mm (300 x 300 DPI)

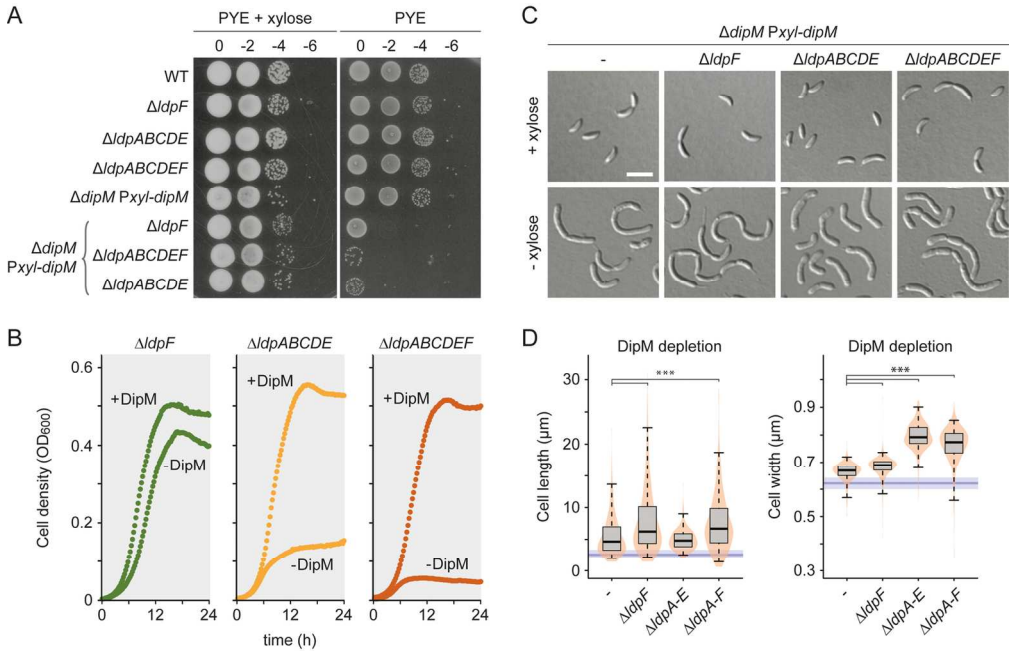

145x94mm (300 x 300 DPI)

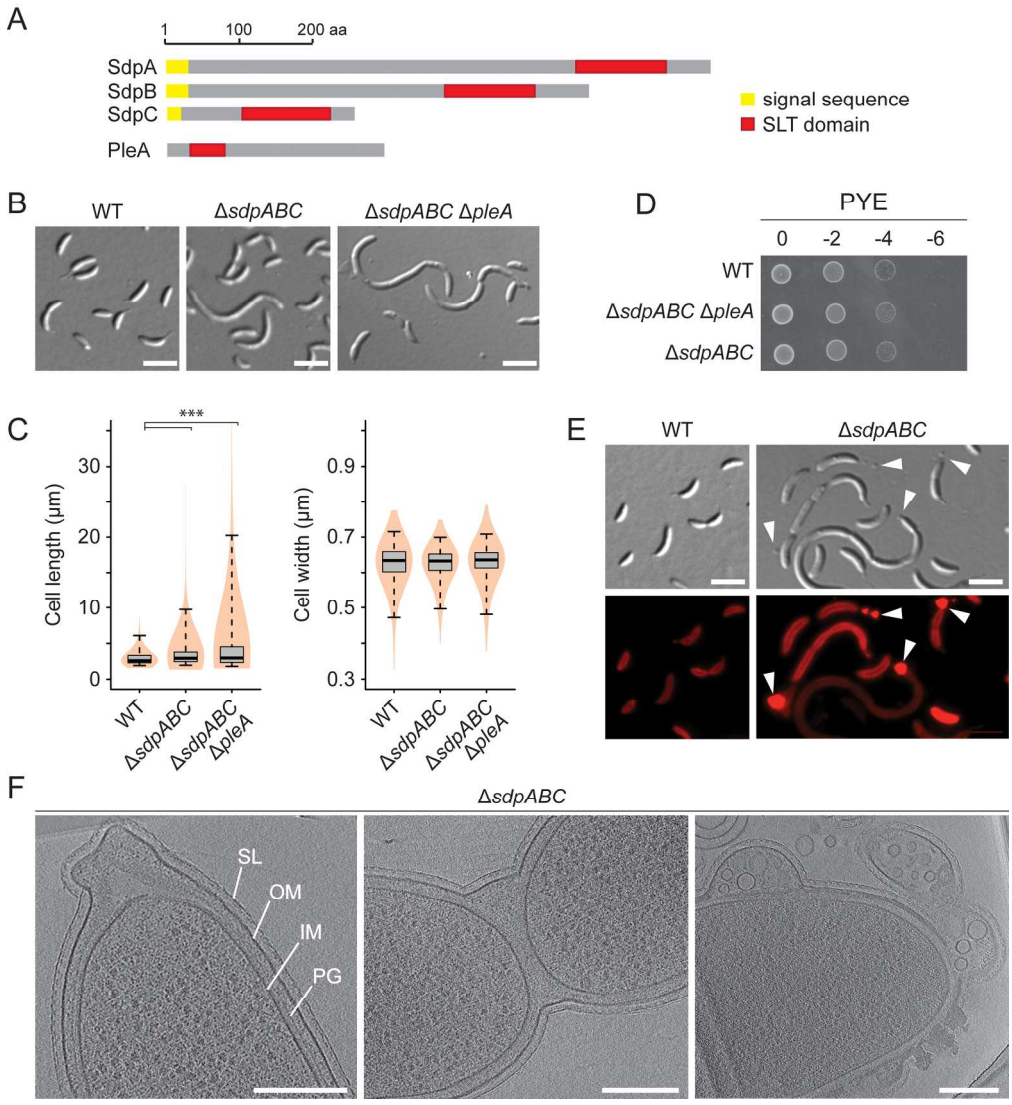

190x208mm (300 x 300 DPI)

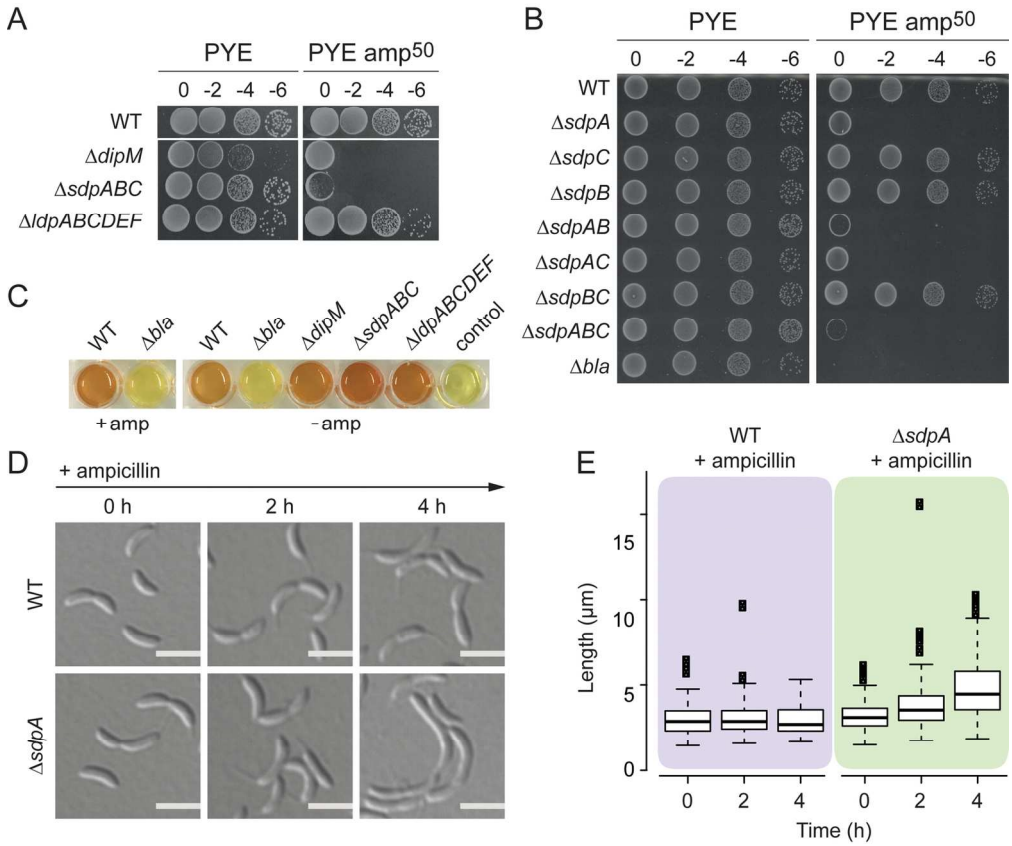

144x121mm (300 x 300 DPI)

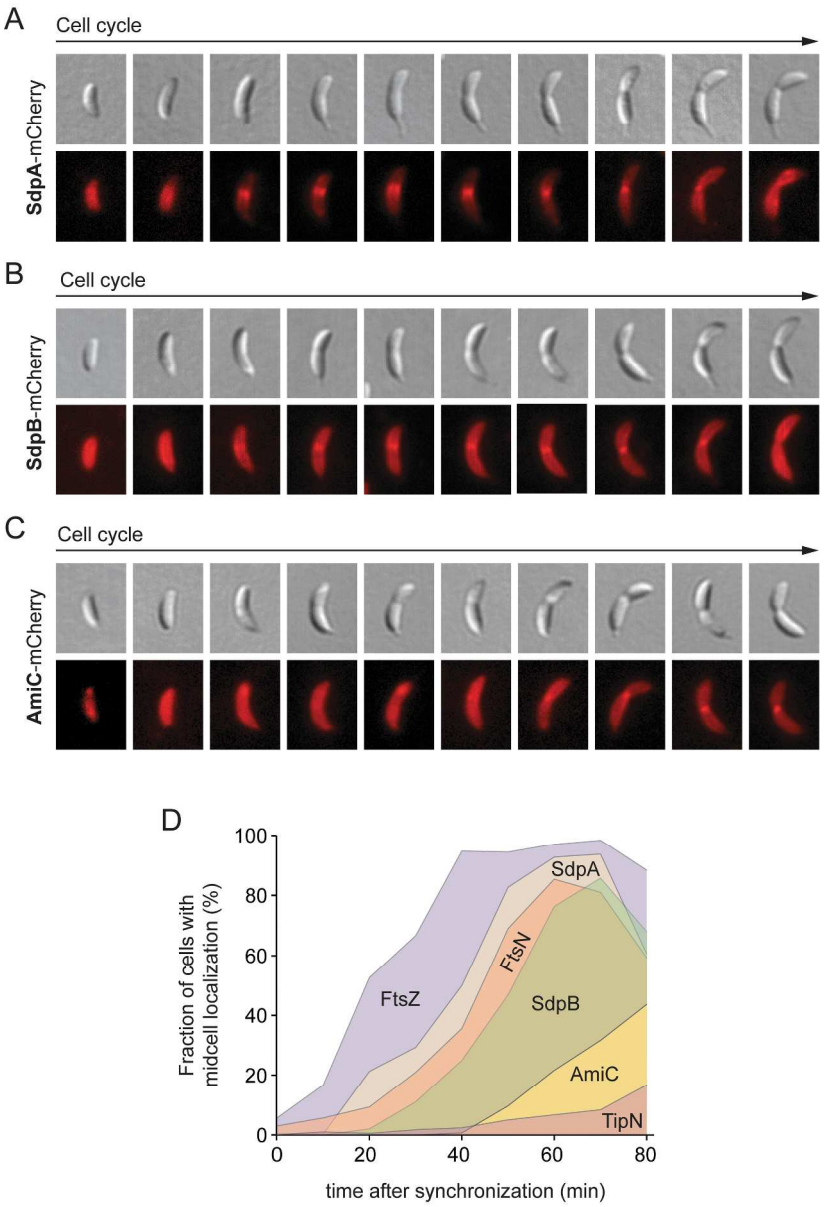

211x311mm (300 x 300 DPI)

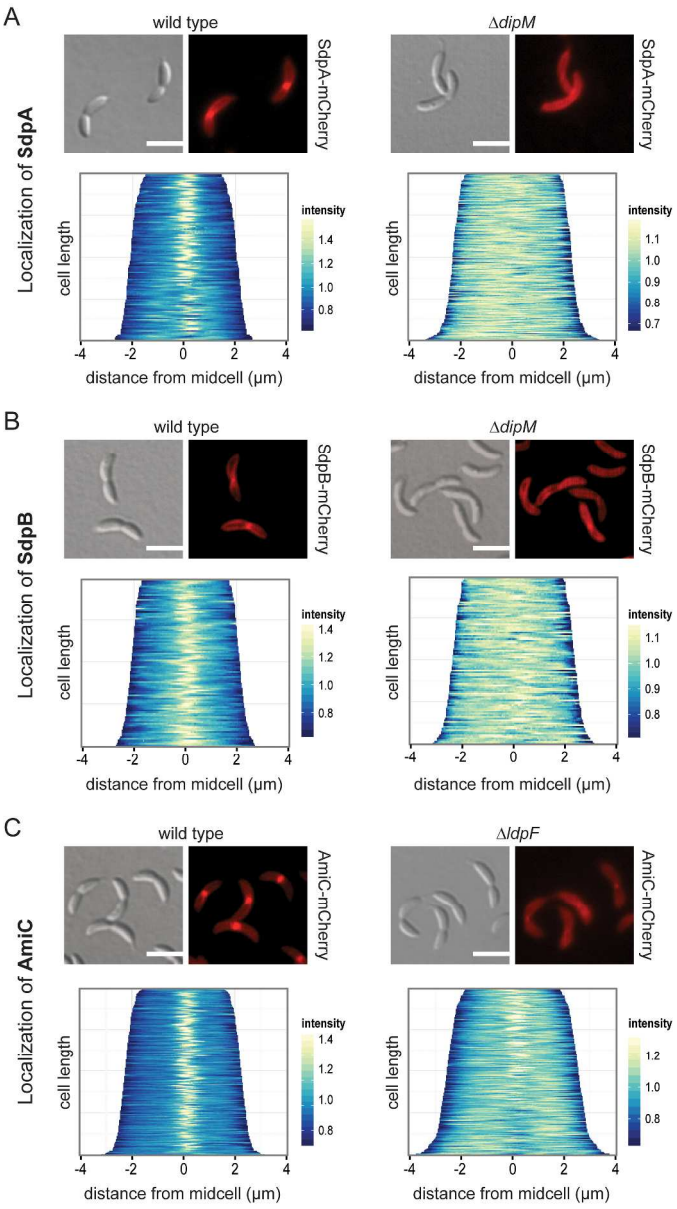

253x454mm (300 x 300 DPI)

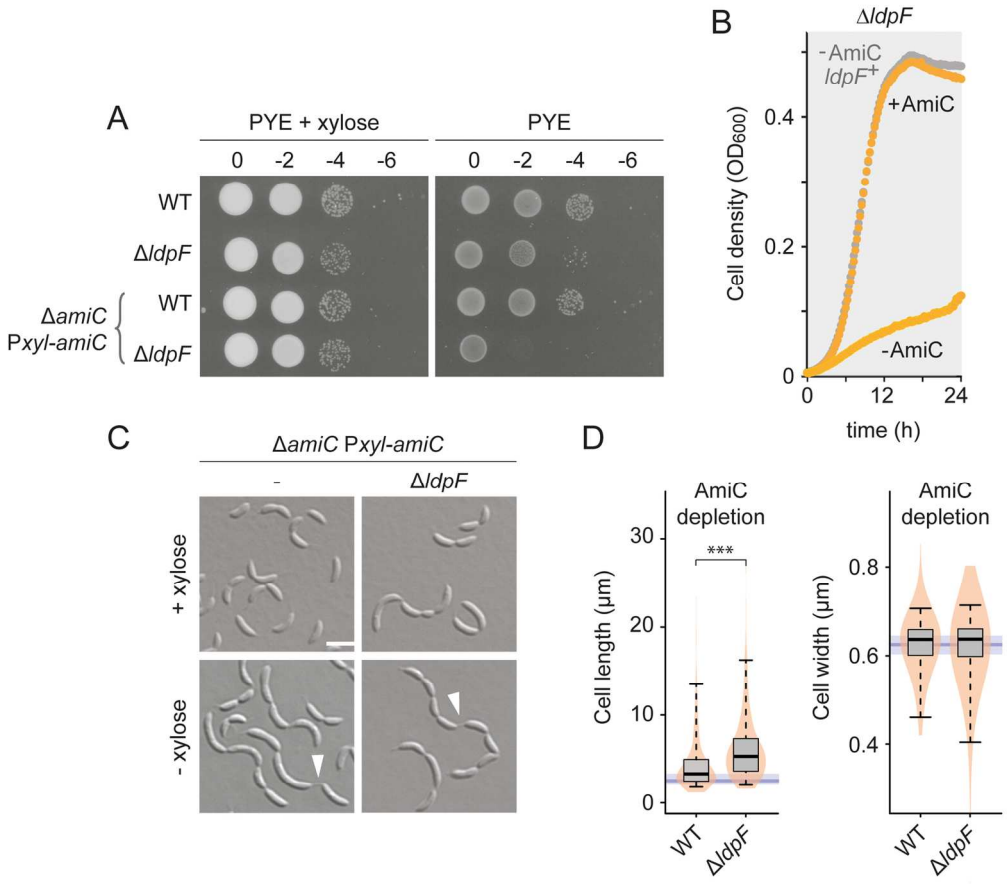

145x130mm (300 x 300 DPI)

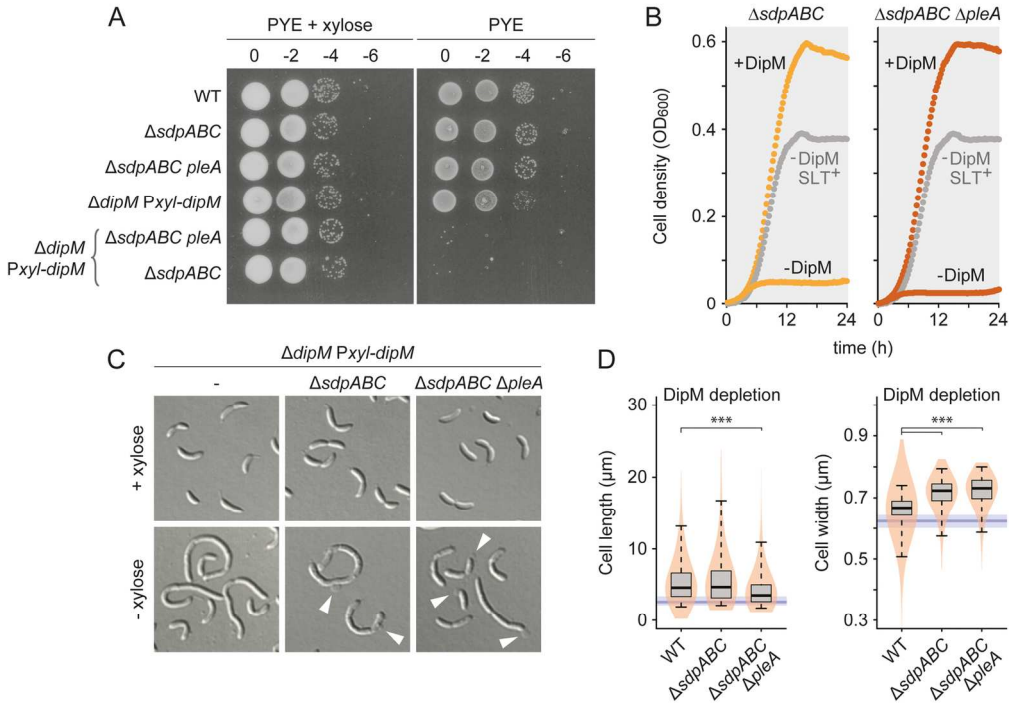

146x106mm (300 x 300 DPI)

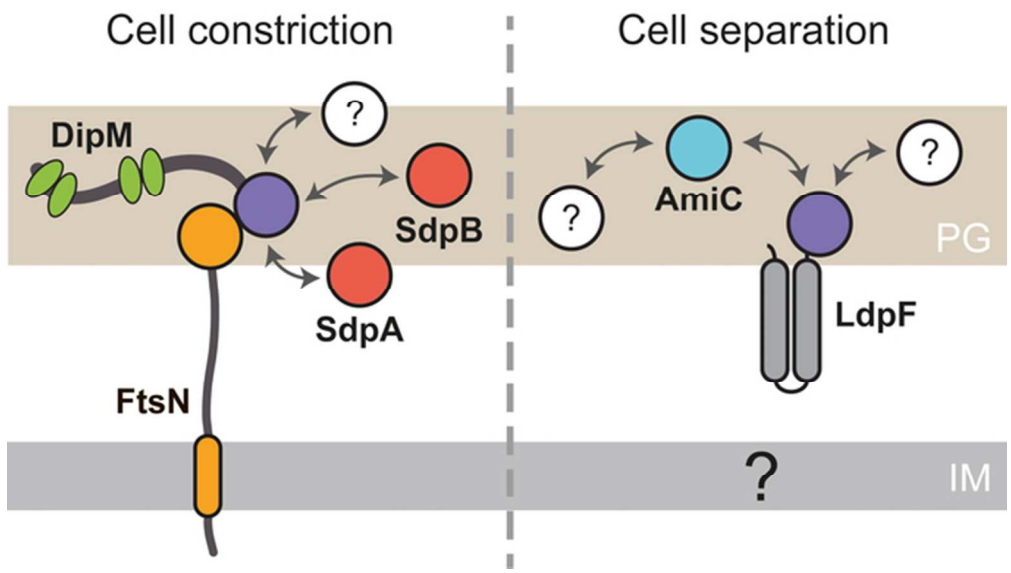

57x32mm (300 x 300 DPI)

Peptidoglycan biosynthesis is mediated by a variety of synthetic and lytic enzymes, whose roles and regulation remain incompletely understood. Here, we comprehensively analyze the autolytic machinery of the alphaproteobacterium *Caulobacter crescentus*. Our study pinpoints factors critical for viability under stress conditions and identifies three more divisome-associated lytic enzymes. Moreover, it reveals two LytM factors with degenerate catalytic domains as regulatory hubs coordinating the activities of multiple peptidoglycan hydrolases during cell constriction and fission, respectively.

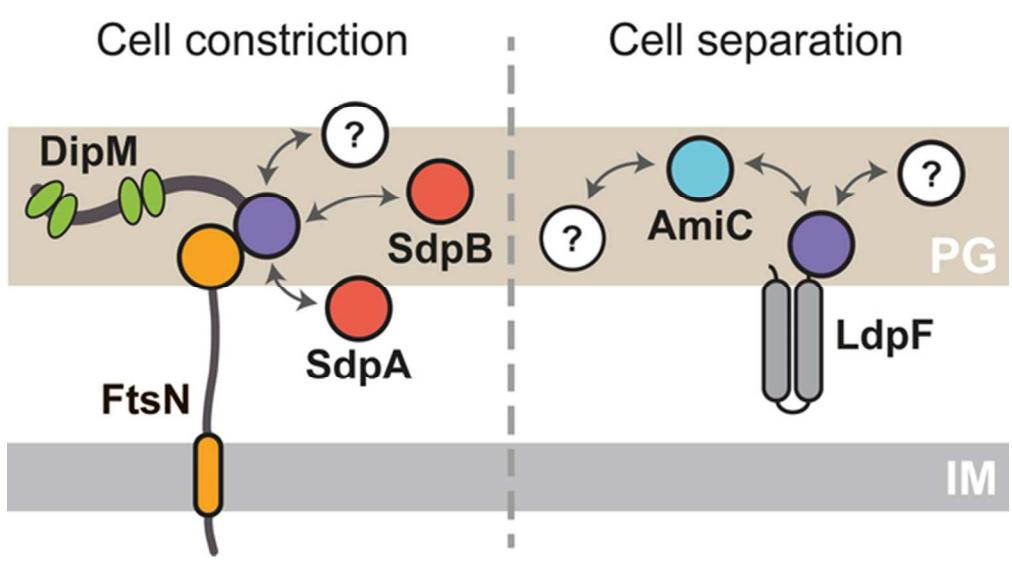

55x29mm (300 x 300 DPI)